

# Spectroelectrochemical Studies of Metalloporphyrins in Room Temperature Ionic Liquid

Yong Soo Hoo  
*Marquette University*

---

## Recommended Citation

Soo Hoo, Yong, "Spectroelectrochemical Studies of Metalloporphyrins in Room Temperature Ionic Liquid" (2010). *Master's Theses (2009 -)*. Paper 52.  
[http://epublications.marquette.edu/theses\\_open/52](http://epublications.marquette.edu/theses_open/52)

SPECTROELECTROCHEMICAL STUDIES OF  
METALLOPORPHYRINS IN ROOM  
TEMPERATURE IONIC LIQUID

by

Yong Soo Hoo, B.A, M.S.

A Thesis Submitted to the Faculty of the Graduate School,  
Marquette University,  
in Partial Fulfillment of the Requirements for  
the Degree of Master of Science

Milwaukee, Wisconsin

August, 2010

ABSTRACT  
SPECTROELECTROCHEMICAL STUDIES OF  
METALLOPORPHYRINS IN ROOM  
TEMPERATURE IONIC LIQUID

Yong Soo Hoo, B.A., M.S.

Marquette University, 2010

The oxidation/reduction reactions of porphyrins and metalloporphyrins play an important role in medicinal, industrial and biochemical reactions<sup>[1]</sup>. Metalloporphyrins are particularly useful as potential catalysts for a variety of processes including catalytic oxidations. The unique properties of metalloporphyrins make them good candidates as electrocatalysts for fuel cells. Metalloporphyrins also play some important roles in biological functions.

By incorporating spectroscopic experiments such as UV-visible or infra-red spectroscopy along with electrochemical experiments such as cyclic voltammetry, one is able to determine the structural changes of the molecule when oxidation or reduction reaction is carried out.

## Table of Contents

List of Figures	iii
List of Tables	v
I. Introduction	1
1.1. Metalloporphyrins	1
1.2. Purpose of using hydrophobic room temperature ionic liquid	14
1.3. Variety of ionic liquids and their properties	16
1.3.1. Viscosity	17
II. Experiments	20
2.1. Equipment	20
2.2. Materials	22
2.3. Procedures	22
2.3.1. Synthesis of 1-Butyl-3-methylimidazolium bromide (BMIMBr) ionic liquid	22
2.3.2. Synthesis of 1-Butyl-3-methylimidazolium hexafluorophosphate (BMIMPF <sub>6</sub> ) ionic liquid	24
III. Results And Discussion	26
3.1. UV-visible studies of metalloporphyrins in ionic liquid	26
3.2. Cyclic Voltammogram (CV) of metalloporphyrins in ionic liquid	32
3.3. Studies done by incorporating CV with UV-visible of metalloporphyrins in ionic liquid	40
3.3.1. Studies done on Co(II)TPP in ionic liquid	40
3.3.1.1. Reason Co(II)TPP is used in our case	40
3.3.1.2. What happens when electrolyte is added into the ionic liquid	41
3.3.1.3. Mixtures of different percentage of Dichloromethane added into ionic liquid as solvent	43

3.3.1.4. Conductivity test done on mixture of various concentration of ionic liquid with $\text{CH}_2\text{Cl}_2$	44
3.3.1.5. Dissolution of $\text{Co(II)TPP}$ in $\text{BMIMBr}$	45
3.3.1.6. $\text{Co(II)TPP}$ oxidized by the ionic liquid under different temperature	48
3.3.2. Studies done on $\text{Mn(III)TPPCl}$ in ionic liquid	52
3.3.2.1. Reduction	52
3.3.2.2. Oxidation	56
3.3.3. Studies done on $\text{Fe(III)TPPCl}$ in ionic liquid	58
3.3.3.1. $\text{Fe(III)TPPCl}$ reduced by ionic liquid	58
3.3.3.2. $\text{Fe(III)TPPCl}$ further reduced by electrochemistry	59
IV. Conclusion	62
References	65

## List of Figures

Scheme 1	Scheme of Co(II)TPP oxidation.	2
Figure 1.1	Time-resolved thin-layer UV-visible spectroelectrochemistry of one-electron oxidation of Co(II)TPP in CH <sub>2</sub> Br <sub>2</sub> -MeCN (1:1) containing 0.1 mol dm <sup>-3</sup> NBu <sub>4</sub> PF <sub>6</sub> .	3
Figure 1.2	Spectroelectrochemical reduction of Mn(TPP)Cl in (A) propylene carbonate and (B) tetrahydrofuran containing 0.1 M Bu <sub>4</sub> NBF <sub>4</sub> .	4
Figure 1.3	Thin-layer spectra recorded before and after controlled-potential reduction at -0.4 V of 5.7 X M Mn(TPP)Cl in ClCH <sub>2</sub> CH <sub>2</sub> Cl containing 0.1 M Bu <sub>4</sub> NBF <sub>4</sub> and (A) 0.0, (B) 0.092 M methanol.	5
Figure 1.4	UV-Visible spectra recorded during thin-layer cyclic voltammetric oxidation of 2.3 X 10 <sup>-4</sup> M Mn(TPP)Cl in ClCH <sub>2</sub> CH <sub>2</sub> Cl containing 0.1M Bu <sub>4</sub> NBF <sub>4</sub> .	6
Figure 1.5	UV-visible adsorption spectrum of Fe(III)TPPCL measured in CHCl <sub>3</sub> at room temperature.	7
Figure 1.6	Summary of overall electron-transfer schemes.	8
Figure 1.7	UV-visible spectral changes observed upon addition of N-methylimidazole to an 8.4X10 <sup>-5</sup> M solution of Fe(III)TPPCL in chloroform.	9
Figure 1.8	UV-visible spectral changes as a function of [Fe(III)TPPCL] in DMF (0.1M TBAP).	11
Figure 1.9	Thin-layer spectra in EtCl <sub>2</sub> for 1X10 <sup>-3</sup> M Fe(III)TPPCL in the presence of 3X10 <sup>-1</sup> M TBAP + 2X10 <sup>-1</sup> M (TBA)Cl at 1) 0.20V, 2) -0.40V, and 3) -0.70V. Reduction of Fe(III) occurs at -0.32V vs SCE.	12
Figure 2.1	Schematic of electrode used in a 5mm UV-visible cell.	21

Figure 2.2	<sup>1</sup> H-NMR of BMIMBr collected using chloroform- <i>d</i> as solvent.	23
Figure 2.3	<sup>1</sup> H-NMR of BMIMPF <sub>6</sub> collected using chloroform- <i>d</i> as solvent.	25
Figure 3.1a	UV-visible spectrum of Fe(III)OEPCl in BMIMBr.	27
Figure 3.1b	UV-visible spectrum of Fe(III)TPPCl in BMIMBr.	28
Figure 3.1c	UV-visible spectrum of Mn(III)TPPCl in BMIMBr.	29
Figure 3.1d	UV-visible spectrum of Fe(III)OEPCl in BMIMPF <sub>6</sub> .	30
Figure 3.1e	UV-visible spectrum of Fe(III)TPPCl in BMIMPF <sub>6</sub> .	31
Figure 3.1f	UV-visible spectrum of Mn(III)OEPCl in BMIMPF <sub>6</sub> .	32
Figure 3.2a	CV of Fe(III)OEPCl in BMIMBr.	34
Figure 3.2b	CV of Fe(III)TPPCl in BMIMBr.	35
Figure 3.2c	CV of Mn(III)OEPCl in BMIMBr.	36
Figure 3.2d	CV of Ferrocene in BMIMBr.	37
Figure 3.3	CV of 0.1mM Co(II)TPP in 30% BMIMPF <sub>6</sub> and 70% CH <sub>2</sub> Cl <sub>2</sub> .	43
Figure 3.4	CV of 0.2mM Co(II)TPP in various percentage of CH <sub>2</sub> Cl <sub>2</sub> in BMIMPF <sub>6</sub> .	44
Figure 3.5	Conductivity test of various percentage of BMIMBr in CH <sub>2</sub> Cl <sub>2</sub> .	45
Figure 3.6	UV-visible spectrum of Co(II)TPP in CH <sub>2</sub> Cl <sub>2</sub> , in BMIMPF <sub>6</sub> after 30 minutes and in BMIMPF <sub>6</sub> while holding the potential of the working electrode at 3500mV.	47
Figure 3.7a	Co(II)TPP oxidized by BMIMBr at 5°C.	49
Figure 3.7b	Co(II)TPP oxidized by BMIMBr at 10°C.	49
Figure 3.7c	Co(II)TPP oxidized by BMIMBr at 15°C.	50
Figure 3.7d	Co(II)TPP oxidized by BMIMBr at 20°C.	50
Figure 3.8	Absorbance change of 434nm peak of Co(II)TPP in BMIMBr at	51

	temperature held at 5, 10, 15, and 20°C.	
Figure 3.9	Arrhenius plot of $\ln(K)$ vs $1/T$ .	52
Figure 3.10	UV-visible spectra of Mn(III)TPPCl while undergoing reduction.	53
Figure 3.11	Reduction reaction of Mn(III)TPPCl. $\lambda_{\max}$ vs E.	54
Figure 3.12	Plot of $\Delta A/\Delta E$ vs. E. Bold line is the raw data. Thin line is the smoothed data where two data points were averaged together.	55
Figure 3.13	CV of reduction reaction of Mn(III)TPPCl in BMIMPF <sub>6</sub> .	56
Figure 3.14	UV-visible spectra of Mn(III)TPPCl while undergoing oxidation reaction.	56
Figure 3.15	Oxidation reaction of Mn(III)TPPCl. $\lambda_{\max}$ vs E.	57
Figure 3.16	UV-visible spectra of Fe(III)TPPCl being reduced by BMIMBr. Spectra were taken every 5 minutes in a vacuum sealed UV cell.	59
Figure 3.17	Time-dependent UV-visible spectra changes obtained during the controlled-potential reduction of Fe(III)TPPCl in BMIMBr.	60
Figure 3.18	Scheme of the prediction of the reduction of Fe(III)TPPCl.	61



## List of Tables

Table 1.1	Comparison of visible spectra for several complexes with Fe(II)TPP.	13
Table 1.2	Typical cation/anion combinations in ionic liquids.	16
Table 1.3	Physical properties and solubilities of commonly used ionic liquids.	16
Table 2.1	Proton chemical shifts for BMIMBr from literature.	24
Table 3.1a	Electrochemical data from the CV of 8mM Fe(III)OEPCl in BMIMPF <sub>6</sub> .	38
Table 3.1b	Electrochemical data from the CV of 8mM Fe(III)TPPCl in BMIMPF <sub>6</sub> .	38
Table 3.1c	Electrochemical data from the CV of 1mM Mn(III)OEPCl in BMIMPF <sub>6</sub> .	38
Table 3.1d	Electrochemical data from the CV of 8mM Ferrocene in BMIMPF <sub>6</sub> .	38

## I. Introduction

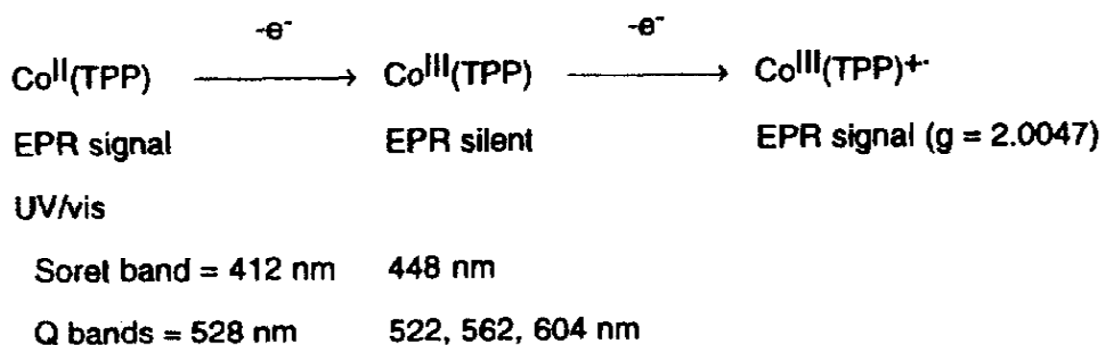
### 1.1. Metalloporphyrins

The oxidation/reduction reactions of porphyrins and metalloporphyrins play an important role in medicinal, industrial and biochemical reactions<sup>[1]</sup>. Metalloporphyrins are particularly useful as potential catalysts for a variety of processes including catalytic oxidations. As global fossil fuel resources are diminishing, considerable attention is being focused on the search for more efficient energy sources. The unique properties of metalloporphyrins make them good candidates as electrocatalysts for fuel cells. Metalloporphyrins also play some important roles in biological functions. For example, heme, a porphyrin which contains iron, is the prosthetic group of a number of major proteins and enzymes<sup>[2]</sup>. These hemoproteins have a variety of biological functions such as storage of oxygen (hemoglobin), activation and transfer of oxygen to substrates (cytochromes P450), and peroxidase reactions. During these processes, the porphyrin molecule serves as an electron source.

Electrochemical experiments are a good tool to use in order to investigate these processes. However, electrochemical experiments lack conclusive information on the electronic structure of the products. To predict the product's electronic structure, spectroscopic evidence is required. To obtain this evidence, spectroelectrochemistry is a wise choice. By incorporating spectroscopic experiments such as UV-visible or infra-red spectroscopy along with electrochemical experiments such as cyclic voltammetry, one is able to determine the structural changes of the molecule when oxidation or reduction reaction is carried out.

Metalloporphyrins, particularly Co(II)TPP, Mn(III)TPPCl and Fe(III)TPPCl, were investigated in our laboratory using spectroelectrochemistry technique with room temperature ionic liquids (RTILs) as solvent. The Co(II)TPP was used as primary investigation for understanding how metalloporphyrins work in ionic liquids. The Co(II)TPP oxidation process is widely known and investigated<sup>[3, 4]</sup> using conventional solvent/electrolyte system. Reported in literature, the oxidation potential of the Co(II)TPP/Co(III)TPP is lower in potential than that of Co(III)TPP/Co(III)TPP<sup>+</sup><sup>[5]</sup>. As a result, Co(II)TPP will be completely oxidized to Co(III)TPP before the oxidation of Co(III)TPP to Co(III)TPP<sup>+</sup> take place. Hence the cyclic-voltammogram(CV) collected will have two distinct oxidation peaks.

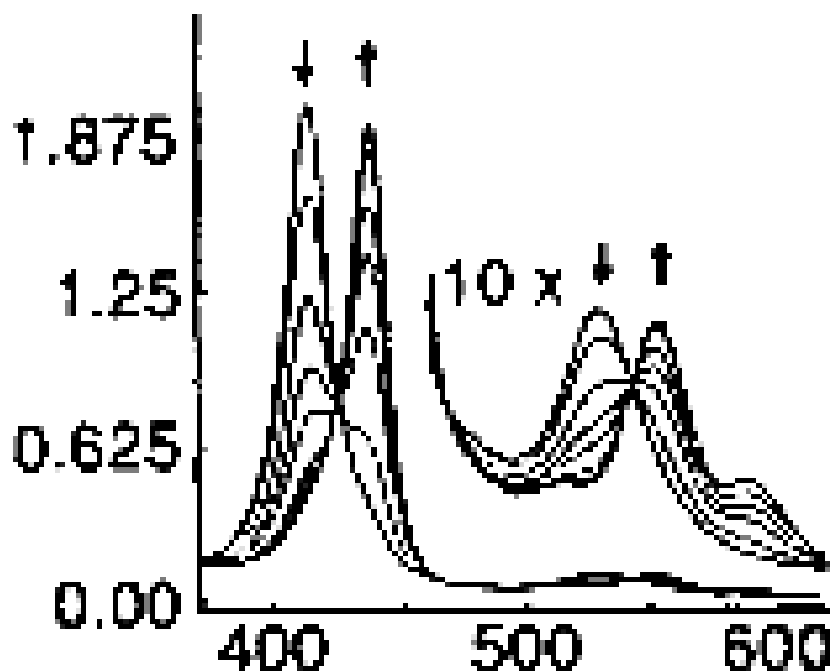
In one of the literature articles reported by Nam *et. al*<sup>[3]</sup>, the oxidation reaction of Co(II)TPP is carried out with dioxygen plus aldehyde. Their UV-visible spectral changes of the cobalt porphyrin complex were summarized in the Scheme 1 shown below.



**Scheme 1. Scheme of Co(II)TPP oxidation<sup>[3]</sup>.**

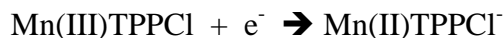
Another report on the UV-visible spectroelectrochemistry is the spectral changes of Co(TPP) during the one electron oxidation, shown in Figure 1.1<sup>[6]</sup>. From the data, one can observe the decrease in the 410 nm Soret band while the 440 nm Soret band

increased in absorbance as the oxidation reaction is carried out. One can also observe the shift of the 537 nm Q band to 612 nm. The spectral changes in Figure 1.1 are relatively close to the one reported in Scheme 1.



**Figure 1.1.** Time-resolved thin-layer UV-visible spectroelectrochemistry of one-electron oxidation of Co(II)TPP in CH<sub>2</sub>Br<sub>2</sub>-MeCN (1:1) containing 0.1 mol dm<sup>-3</sup> NBu<sub>4</sub>PF<sub>6</sub><sup>[6]</sup>.

Mn(III)TPPCl was found to undergoes a quasi-reversible one electron reduction at around -250mV. In a non-coordinating solvent, e.g. CH<sub>2</sub>Cl<sub>2</sub>, the axial Cl<sup>-</sup> ligand is bound to the metal in both oxidation states<sup>[7]</sup>. The electrode reaction is shown as below.



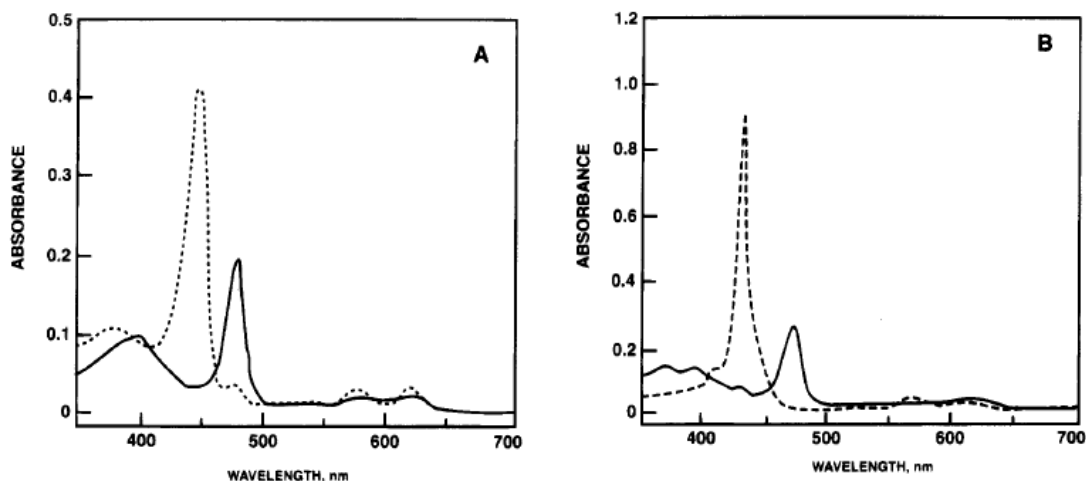


**Figure 1.2. Spectroelectrochemical reduction of Mn(TPP)Cl in (A) propylene carbonate and (B) tetrahydrofuran containing 0.1 M Bu<sub>4</sub>NBF<sub>4</sub>. Working electrode potential: 0.0 V (-); -0.5 V (- - -)<sup>[7]</sup>.**

Figure 1.2 above shows the spectroelectrochemical reduction of Mn(III)TPPCl in propylene carbonate and tetrahydrofuran containing 0.1M Bu<sub>4</sub>NBF<sub>4</sub> done by Mu and Schultz<sup>[7]</sup>. At a potential of 0mV, the Mn(III) complex shows the Soret band at 476nm while two other Q bands at 582 and 620 nm. The 476 nm Soret band was found to shift to 442nm when the potential was held at -500mV. By comparing the ratio of the Q band to the Soret band, the authors claimed that, during the reduction process, the Cl<sup>-</sup> is still bounded to the metal center. As a result, the Mn(III) and Mn(II) species exist in the solution are Mn(III)TPPCl and Mn(II)TPPCl<sup>-</sup>.

Also reported by the same authors, the UV-visible spectra change for the reduction of Mn(III)TPPCl to Mn(II)TPPCl<sup>-</sup> when the electrode potential is held at -400mV<sup>[8]</sup>. The results are shown in Figure 1.3.

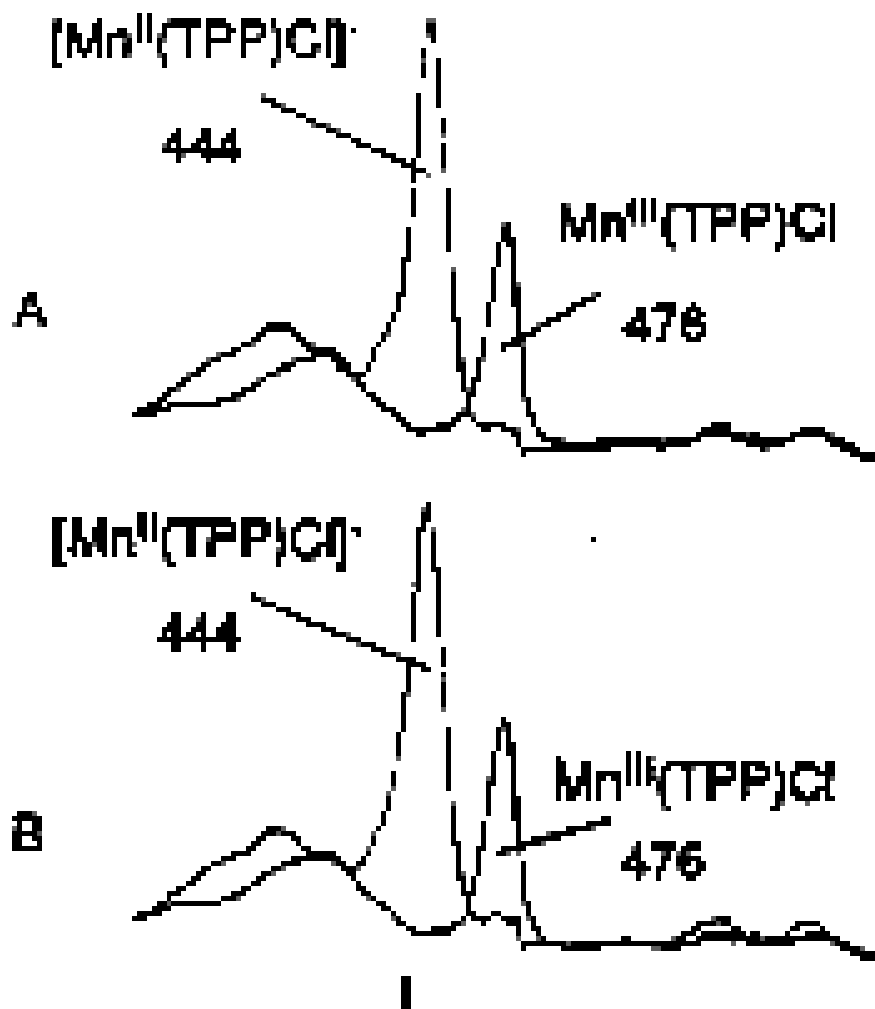
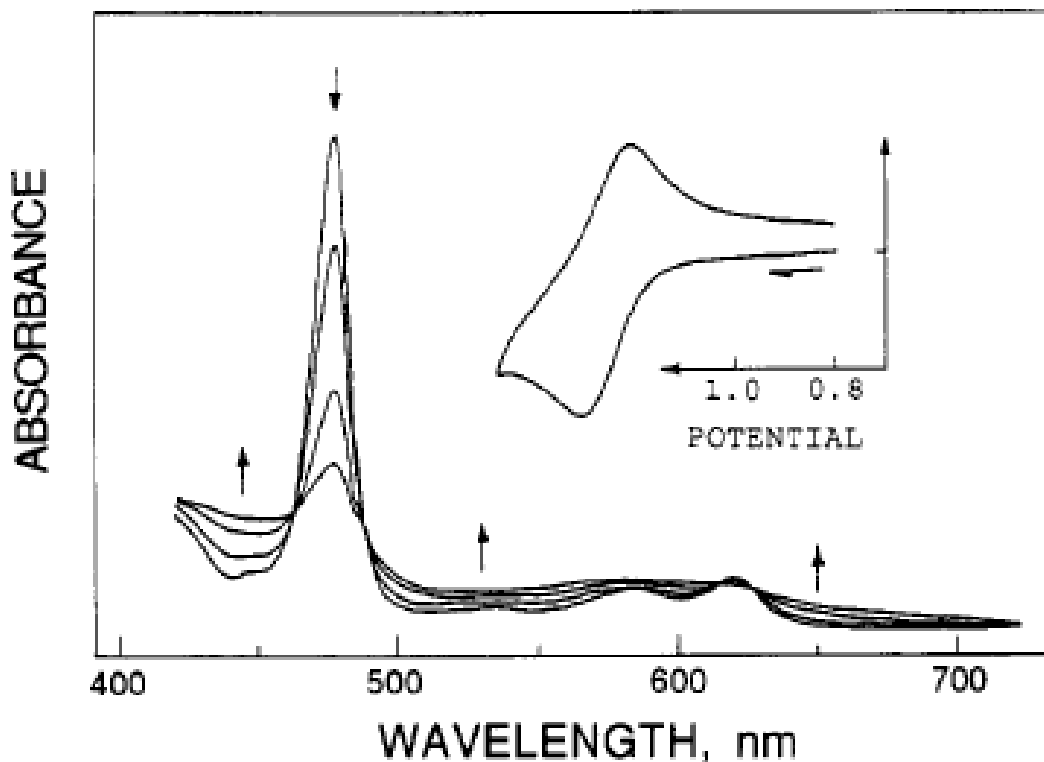


Figure 1.3. Thin-layer spectra recorded before and after controlled-potential reduction at -0.4 V of  $5.7 \times 10^{-5} M$   $Mn(TPP)Cl$  in  $ClCH_2CH_2Cl$  containing 0.1 M  $Bu_4NBF_4$  and (A) 0.0, (B) 0.092 M methanol<sup>[8]</sup>.

Oxidation of  $Mn(III)TPPCl$  is also of interest to us. Reported by Mu and Schultz<sup>[8]</sup> in the same article, Figure 1.4 show the UV-visible spectra taken while  $Mn(III)TPPCl$  undergoes oxidation process during CV. From the figure, we see that when  $Mn(III)TPPCl$  undergoes oxidation process, the 476nm Soret band decreased in

intensity and the peak shape broaden, while the baseline of the UV-visible spectra also increased.



**Figure 1.4.** UV-Visible spectra recorded during thin-layer cyclic voltammetric oxidation of  $2.3 \times 10^{-4}$  M Mn(TPP)Cl in  $\text{ClCH}_2\text{CH}_2\text{Cl}$  containing 0.1M BudNBF<sub>4</sub>. Inset: Thin-layer cyclic voltammogram recorded at a sweep rate of  $5 \text{ mV s}^{-1}$ .

Among the wide range of metalloporphyrins available, iron porphyrin is possibly the most difficult to understand. There are generally three types of electronic transitions for iron porphyrins: porphyrin to metal charge-transfer, electron transfer from axially coordinated ligand to iron charge-transfer, and porphyrin  $\pi \rightarrow \pi^*$  transitions.

Shown in Figure 1.5 is a typical UV-visible spectrum of Fe(III)TPPCl in  $\text{CHCl}_3$  at room temperature. When the reduction process is carried out, the ferric complex was

reduced to a ferrous complex. It is well known that the redox reaction of the five-coordinated high spin Fe(III) complexes (i.e. Fe(III)OEPCl and Fe(III)TPCl) depends upon the solvent counterion<sup>[9]</sup>. If one takes account of the possible spin states of every reactant and their reduced product, there are nine different types of electron-transfer reaction<sup>[9]</sup>. High spin Fe<sup>III</sup> may be reduced to high, intermediate, or low spin Fe<sup>II</sup>. Where intermediate Fe<sup>III</sup> may be reduced to high, intermediate, or low spin Fe<sup>II</sup>. Lastly, low spin Fe<sup>III</sup> may be reduced to high, intermediate, or low spin Fe<sup>II</sup>. However, due to the known chemistry of the iron porphyrin system, 3 electrode reactions are generally observed, which is high spin Fe<sup>III</sup> to high spin Fe<sup>II</sup>, intermediate Fe<sup>III</sup> to intermediate Fe<sup>II</sup>, and low spin Fe<sup>III</sup> to low spin Fe<sup>II</sup>.

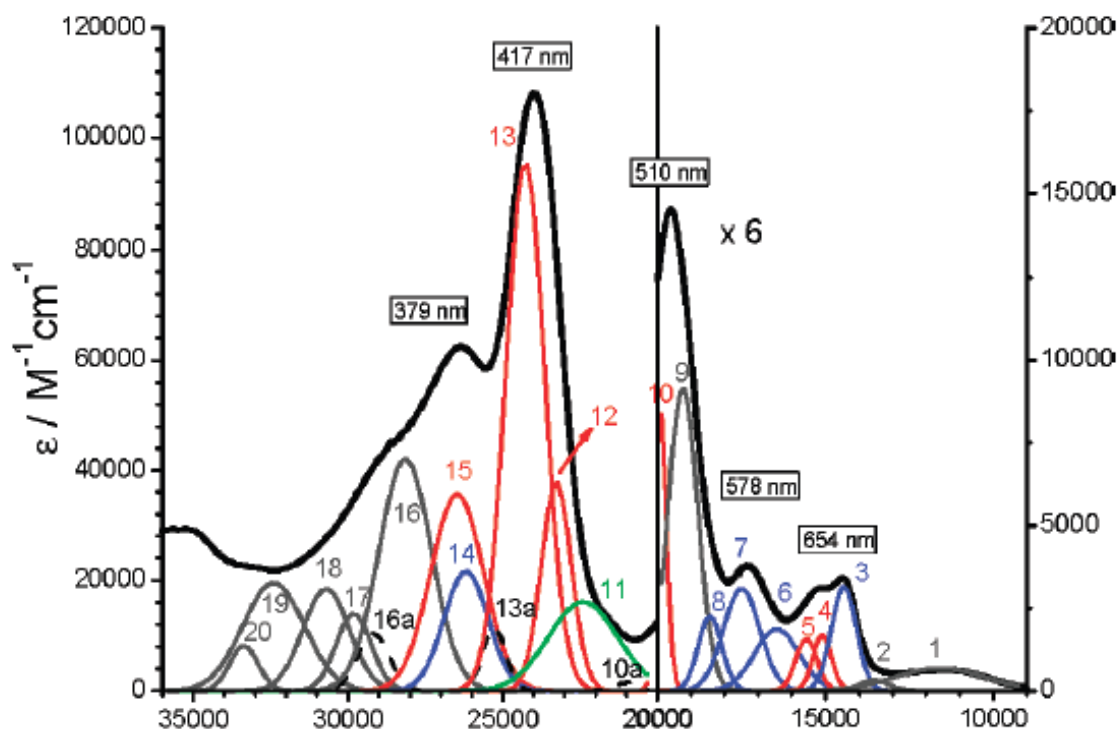


**Figure 1.5.** UV-visible adsorption spectrum of Fe(III)TPPCl measured in CHCl<sub>3</sub> at room temperature<sup>[10]</sup>.



Shown in Figure 1.6 is a general reduction reaction mechanism of iron(III) porphyrin to iron(II) porphyrins. Depending on the solvent (S= DMF, DMSO, etc) used and the nature of X (X=Cl<sup>-</sup>, Br<sup>-</sup>, N<sub>3</sub><sup>-</sup>, F<sup>-</sup>, etc), the electrode products formed can be different. For example, a reactant Fe(III)TPPX can be reduced to either [Fe(II)TPPX]<sup>-</sup>, Fe(II)TPP(S), or [Fe(II)TPPX(S)]<sup>-</sup>. In our case, we will focus on the iron porphyrin where X is a halide. When an anion like Cl<sup>-</sup> binds to iron porphyrin, the resulting reactant are usually a high-spin Fe(III) complexes. As mention above, it had been generally found that the iron porphyrin system, high-spin Fe<sup>III</sup> will be reduced to high-spin Fe<sup>II</sup>. For example reduction of Fe(III)TPPCl or Fe(III)TPPBr will yield high-spin [Fe(II)TPPX]<sup>-</sup> as initial product, and the ultimate Fe(II) complex is the Fe(II)TPP. The reason X was used in the initial product is because it is well-known that the original axial ligand can be easily replaced in iron porphyrin complex <sup>[9, 11-17]</sup>.

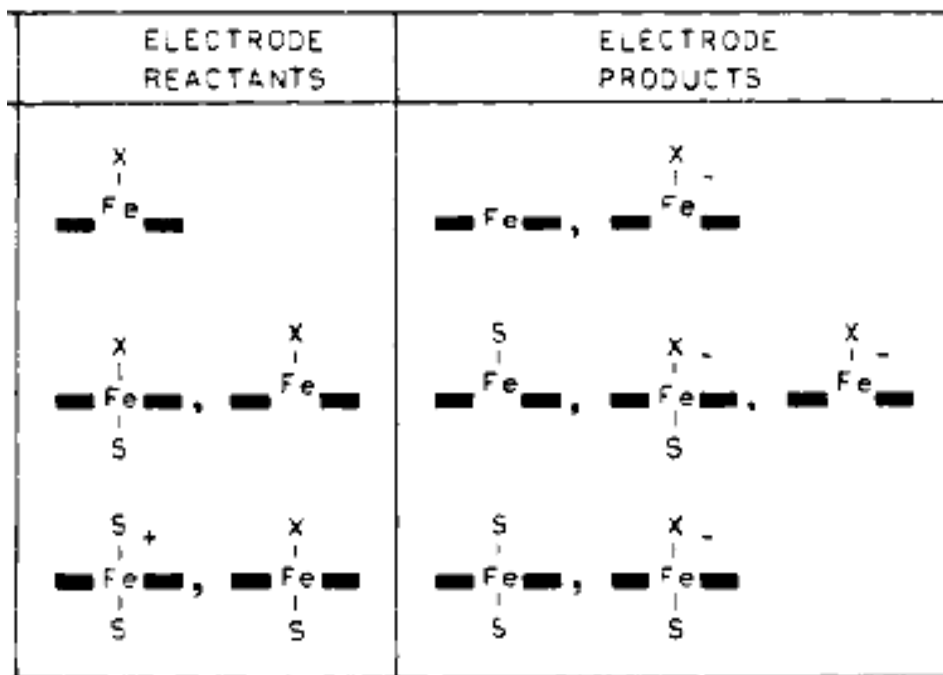
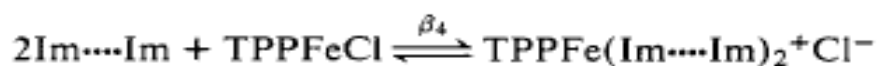


Figure 1.6. Summary of overall electron-transfer schemes<sup>[9]</sup>.

Shown in Figure 1.7 is a UV-visible spectral changes of an  $8.4 \times 10^{-5}$  M Fe(III)TPPCL in chloroform when N-methylimidazole is added to the solution<sup>[16]</sup>. The authors claimed that addition of amine (in their case N-methylimidazole) can lead to the dissociation of the halide ion bounded to the iron center of the iron porphyrin complexes. Suggested by the authors that addition of higher concentration of N-methylimidazole will lead to the reaction shown below:



The authors also reported that when this reaction is carried out, the chloride ion is found to be hydrogen bonded to one of the imidazole N-H groups.

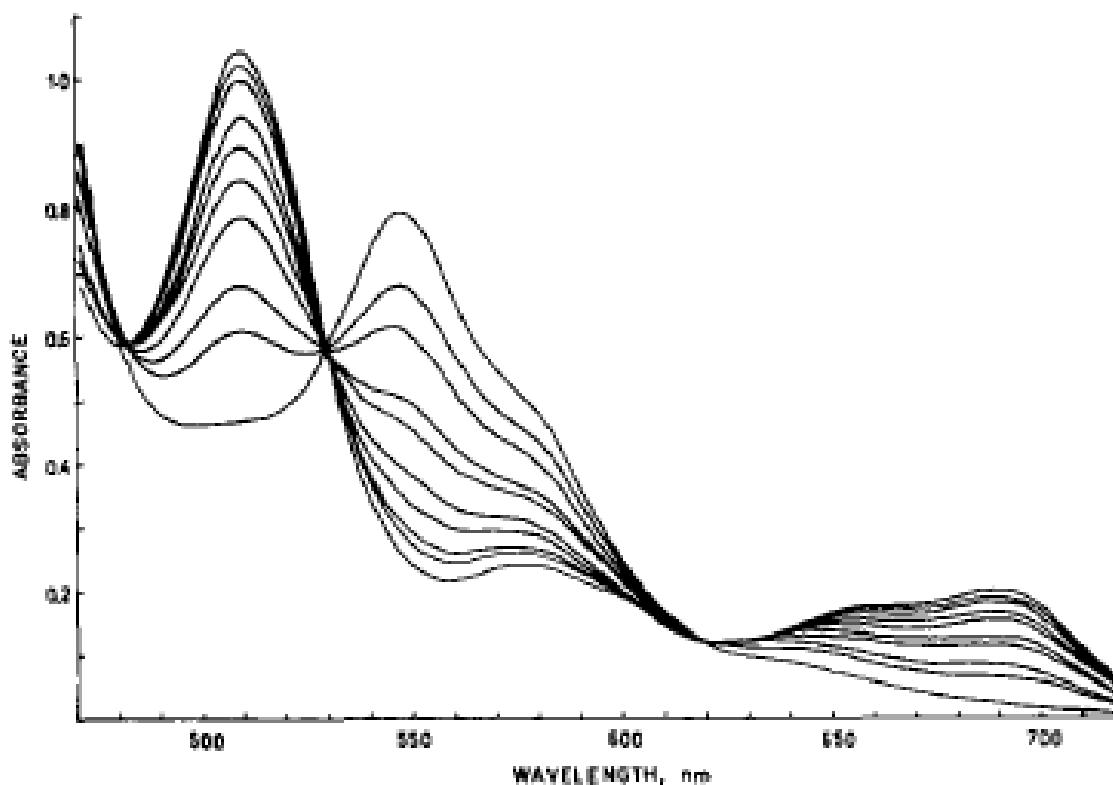
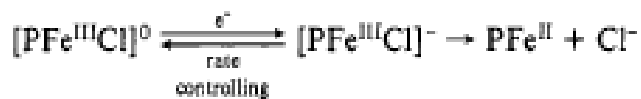
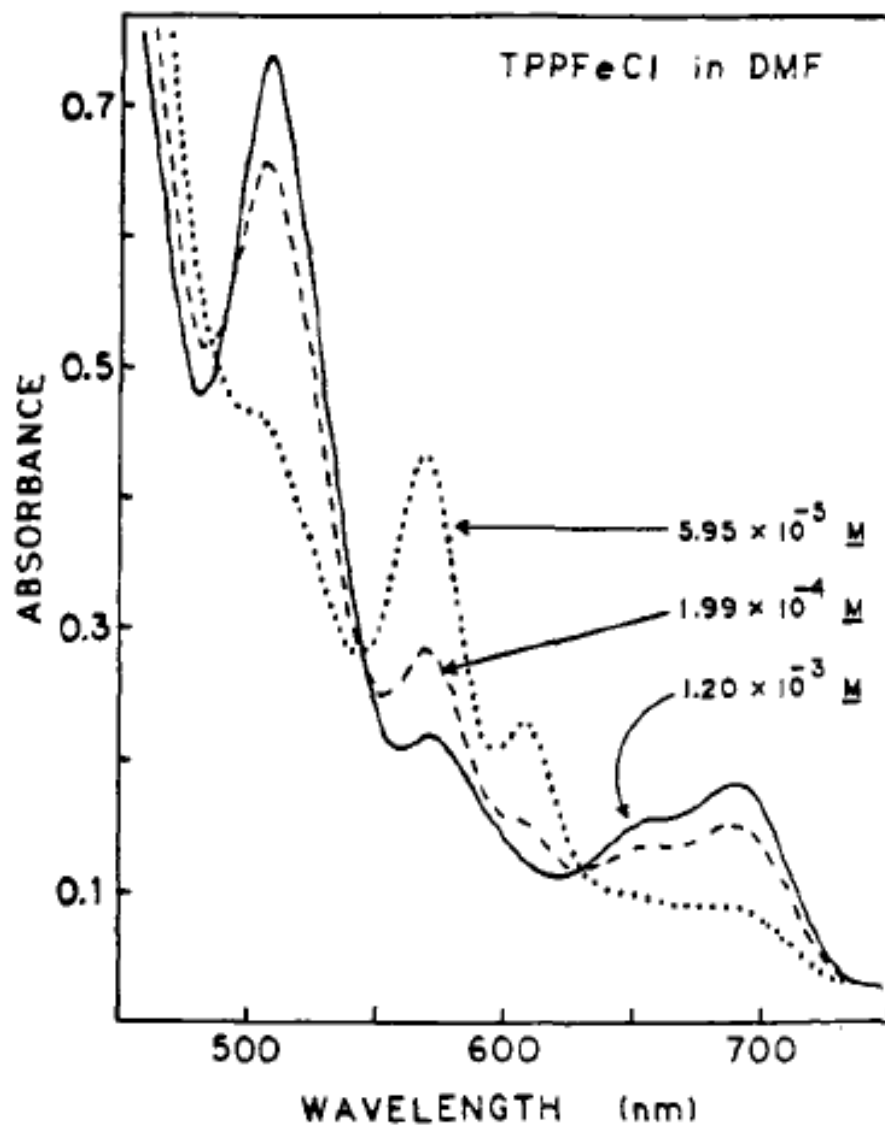


Figure 1.7. UV-visible spectral changes observed upon addition of N-methylimidazole to an  $8.4 \times 10^{-5}$  M solution of Fe(III)TPPCL in chloroform<sup>[16]</sup>.

Reported by different authors, Shantha *et. al.*, also observed the similar UV-visible spectral changes when 1,2-dimethylimidazole (1,2-Me<sub>2</sub>Im)(L<sub>1</sub>) was added into the Fe(III)TPPCl solution. The authors reported that the disappearance of the 370nm and 510nm bands (which are characteristic of coordinated chloride iron species), leads them to believe that the discrepancy is due to the formation of the 5-coordinated [Fe(TPP)(L<sub>1</sub>)]<sup>+</sup>Cl<sup>-</sup> iron(III) complex<sup>[11]</sup>. If the reaction is carried out in chloroform, which has a higher equilibrium constant that is capable of H bonding, a more complete depolymerization of the imidazole will occurs where the formation of [Fe(TPP)(L<sub>1</sub>)<sub>2</sub>]<sup>+</sup>Cl<sup>-</sup> species occurred.

Kadish *et. al.* reported in three separate articles, from 1980 to 1983, on the influence of counterion and solvent effects on the electrode reaction of iron porphyrins<sup>[12, 13, 17]</sup>. At lower [Fe(III)TPPCl], the Cl<sup>-</sup> will dissociate (shown in Figure 1.8), when a coordinating solvent such as THF is used. Thus, the THF can coordinate one solvent molecule to the iron center of Fe(III)TPPX where X= Cl<sup>-</sup>, Br<sup>-</sup>, N<sub>3</sub><sup>-</sup> and F<sup>-</sup>, where if X=ClO<sub>4</sub><sup>-</sup>, then two solvent molecules will bind to the iron center. The reactant at the electrode surface would be either Fe(III)TPPX(THF) or Fe(III)TPP(THF)<sub>2</sub><sup>+</sup>ClO<sub>4</sub><sup>-</sup>. Proposed by the authors is a mechanism of the reduction reaction on the electrode, shown in the equation below:





**Figure 1.8.** UV-visible spectral changes as a function of [Fe(III)TPPCl] in DMF (0.1M TBAP)<sup>[13]</sup>.

Shown in Figure 1.9 is the thin-layer UV-visible spectra of reduction reaction of Fe(III)TPPCl. The spectra in solutions that contain additional halide ion show the presence of a species other than just Fe(II)TPP due to the appearance of the 570nm and 610nm peaks. Initial proposal was that these peaks could be due to dimerization of

Fe(II)TPP to  $[\text{Fe(II)TPP}]_2\text{O}$ . However, after comparing with the data shown in Table 1.1, the authors came to the conclusion that the unknown species could be  $[\text{Fe(II)TPPX}]^-$  or the well-known five coordinate, high-spin Fe(II)TPP(L) where L is a sterically hindered ligand.

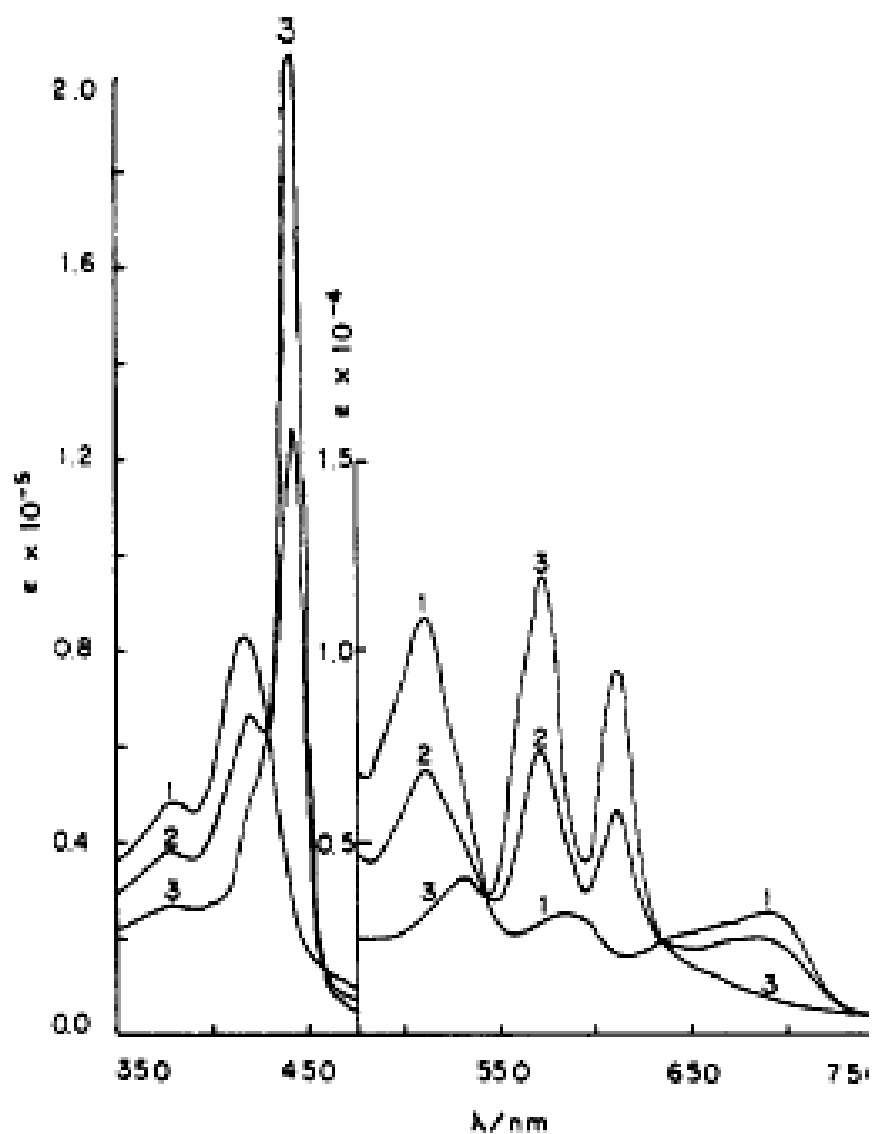


**Figure 1.9.** Thin-layer spectra in  $\text{EtCl}_2$  for  $1 \times 10^{-3}$  M Fe(III)TPP in the presence of  $3 \times 10^{-1}$  M TBAP +  $2 \times 10^{-1}$  M (TBA)Cl at 1) 0.20V, 2) -0.40V, and 3) -0.70V. Reduction of Fe(III) occurs at -0.32V vs SCE.

**Table 1.1. Comparison of visible spectra for several complexes with Fe(II)TPP<sup>[17]</sup>.**

**Sh = shoulder.**

complex	solvent	Soret max, nm ( $10^{-4} \epsilon$ )	other maxima in visible region, nm ( $10^{-4} \epsilon$ ) <sup>a</sup>			
(TPP)Fe	benzene	420 (9.6)	445 (7.0)	540 (1.0)		
(TPP)Fe	EtCl <sub>2</sub>	417 (8.0)	443 (6.5)	537 (0.9)		
(TPP)FeF <sup>-</sup>	EtCl <sub>2</sub>	441 (22.9)		530 sh (0.48)	570 (1.2)	610 (0.89)
(TPP)FeCl <sup>-</sup>	EtCl <sub>2</sub>	441 (20.5)		530 sh (0.53)	570 (1.2)	610 (0.84)
(TPP)FeOAc <sup>-</sup>	EtCl <sub>2</sub>	441 (18.3)		530 sh (0.51)	570 (1.0)	610 (0.66)
(TPP)FeBr <sup>-</sup>	EtCl <sub>2</sub>	441 (18.9)		530 sh (0.48)	570 (1.1)	610 (0.74)
(TPP)Fe(2-MeImH)	EtCl <sub>2</sub>	437 (17.6)		534 (0.74)	565 (0.82)	606 (0.46)
(TPP)Fe(2-MeIm) <sup>-</sup>	THF	446 (11.0)		530 (0.7)	573 (1.7)	614 (1.5)
(TPP)Fe(ImH) <sub>2</sub>	EtCl <sub>2</sub>	426 (24.0)		534 (2.0)	565 (0.6)	
(TPP)Fe(Me <sub>2</sub> SO) <sub>2</sub>	Me <sub>2</sub> SO	428 (17)		532 (0.95)	561, 602 sh	

From the data reported up to this point, the electroreduction of neutral, synthetic iron(III)porphyrins containing axially coordinated halides form a negatively charged halide-bound Fe(II) complex which can be found as the initial product, before fully converted to Fe(II)TPP.

## 1.2. Purpose of using hydrophobic room temperature ionic liquid

A room temperature ionic liquid (RTIL) is defined as a material in which only ionic species are present in the solution with a melting temperature below 398K. RTIL is usually formed with a bulky organic cation that weakly interacts with an inorganic anion<sup>[18]</sup>. The use of ionic liquids in electrochemical and organic synthesis has been widely investigated in the past few years<sup>[19-22]</sup>. Due to their ionic conductivity, low volatility, high chemical and thermal stability, low combustibility, and high-quality solvating properties for most organic compounds, ionic liquids have been highly accepted in the electrochemistry field<sup>[23, 24]</sup>. Since the discovery of 1-ethyl-3-methylimidazolium chloroaluminates reported by Wilkes *et. al*<sup>[25]</sup>, ionic liquids have been shown to have a broad electrochemical window of more than 3V. As a result, electrochemical experiments have gradually evolved from using conventional organic solvent/supporting electrolyte system into this non-volatile system. By using ionic liquids, one can decrease the emission of organic solvents into the environment since the vapor pressure of the ionic liquids is almost negligible.

Another important aspect of RTILs that is widely accepted is due to their abundance of charge carriers. Hence, RTILs can be used as solvents without the need of added electrolytes which, in return, minimizes waste<sup>[26]</sup>. Since the use of electrolyte can be eliminated, the RTILs can also be easily recycled. As a result, this will cut down the cost of expensive electrolyte and reduced the waste of solvent when running electrochemical experiments.

However, the real advantage to using RTILs is not entirely due to its intrinsic conductivity but to its low volatility. Even though the RTILs are made entirely of ionic

species, the conductivities are close to the traditional solvents with supporting electrolytes added. The reason for this phenomenon is due to its high viscosity. As a result, RTILs are named “green solvents” because of their low volatility.

In many cases, not all ionic liquids are useful in the practical sense if the melting points of the salts are too high. On the other hand, some ionic liquids are free flowing at room temperature. These ionic liquids are called *ambient temperature ionic liquids*. Given that one is able to “tune” the solvent using a variety of the cations and anions in order for a specific purpose, RTILs are also given the name “designer solvents”<sup>[27, 28]</sup>.

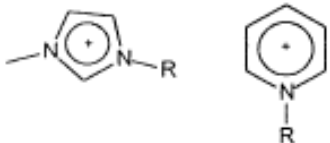
In the electrochemical field, RTILs have been used as solvents in many different applications such as solar cells, fuel cells, sensors, capacitors, and lithium batteries<sup>[29]</sup>. Due to the characteristic of ionic liquids being able to sustain high temperature and pressure changes while remaining physically and chemically unchanged, they can be used as the electrolyte in gas sensors. Conventional electrolytes when used in gas sensors (e.g. H<sub>2</sub>SO<sub>4</sub>/H<sub>2</sub>O), rely on water which is volatile and over time evaporates, thus, shortening the lifetime of the sensor<sup>[30]</sup>.



### 1.3. Variety of ionic liquids and their properties

Room Temperature Ionic Liquids are typically formed from organic nitrogen-containing heterocyclic cations and inorganic anions. Table 1.2 (shown below) contains some examples of combinations of cations and anions which are typically used in synthesizing ionic liquids. Table 1.3 shows the physical properties of some commonly used ionic liquids.

**Table 1.2. Typical cation/anion combinations in ionic liquids, taken from reference [19].**

Cations <sup>a</sup>	Anions
	$[\text{BF}_4]^-$ , $[\text{PF}_6]^-$ , $[\text{SbF}_6]^-$ , $[\text{CF}_3\text{SO}_3]^-$ , $[\text{CuCl}_2]^-$ , $[\text{AlCl}_4]^-$ , $[\text{AlBr}_4]^-$ , $[\text{AlI}_4]^-$ , $[\text{AlCl}_3\text{Et}]^-$ , $[\text{NO}_3]^-$ , $[\text{NO}_2]^-$ , $[\text{SO}_4]^{2-}$
$\text{PR}_4^+$ , $\text{SR}_4^+$ , $\text{NR}_4^+$	$[\text{Cu}_2\text{Cl}_3]^-$ , $[\text{Cu}_3\text{Cl}_4]^-$ , $[\text{Al}_2\text{Cl}_7]^-$ , $[\text{Al}_3\text{Cl}_{10}]^-$

<sup>a</sup> R = alkyl.

**Table 1.3. Physical properties and solubilities of commonly used ionic liquids, taken from reference [19].**

Ionic liquid <sup>a</sup>	$\lambda^b$	MW (g/mol)	Color (with impurities)	Density (g/ml)	Liquid temperature (°C)		Solubility in common solvents <sup>c</sup>							
					Lowest	Highest	Water	Methanol	Acetone	Chloroform	Petroleum ether	Hexane	Acetic anhydride	Toluene
[bmim]BF <sub>4</sub>		226.02	Light yellow	1.320	-48.96	399.20	s	s	s	s	i	i	i	i
[bmim]PF <sub>6</sub>		284.18	Light yellow	1.510	13.50	388.34	i	s	s	s	i	i	s	i
[bmim]Cl/AlCl <sub>3</sub>	0.50	154.01	Light brown	1.421	-88.69	263.10	r	r	s	s	i	i	s	s
	0.55	151.94	Light brown	1.456	-94.44	286.59	r	r	s	s	i	i	s	s
	0.60	149.87	Light brown	1.481	-95.87	316.34	r	r	s	s	i	i	s	s
[emim]Br/AlCl <sub>3</sub>	0.50	162.21	Purplish black	1.575	13.61	272.51	r	r	s	i	i	i	s	i
	0.55	159.32	Brownish black	1.656	6.45	294.02	r	r	s	i	i	i	s	i
	0.60	156.43	Brownish black	1.995	-19.08	345.34	r	r	s	i	i	i	s	i
[emim]PF <sub>6</sub>		256.13	Yellow	1.426	2.71	304.65	i	i	s	s	i	i	s	i
N-butylpyridine/AlCl <sub>3</sub>	0.50	152.50	Yellow	1.412	18.80	240.00	r	r	s	i	i	i	s	s
	0.55	150.59	Brownish yellow	1.430	33.73	245.39	r	r	s	i	i	i	s	s
	0.60	148.67	Brownish yellow	1.497	18.11	260.24	r	r	s	i	i	i	s	s
(CH <sub>3</sub> ) <sub>3</sub> NHCl/2AlCl <sub>3</sub>	0.66	362.25	Brownish yellow	1.621	-67.90	80.25	r	r	s	i	i	i	s	s

<sup>a</sup> [bmim] = 1-butyl-3-methylimidazolium, [emim] = 1-ethyl-3-methylimidazolium.

<sup>b</sup> Apparent mole fraction of AlCl<sub>3</sub>.

<sup>c</sup> s: soluble, i: insoluble, r: may react with each other.

### 1.3.1. Viscosity

In an electrochemistry experiment, viscosity of a solvent plays an important role. As the viscosity of the solvent increases, the rate of reaction will slow down, especially when the reaction is diffusion controlled<sup>[31]</sup>. For example, in large molecules such as ferrocene, the diffusion coefficient is found to be inversely proportional to the viscosity as shown in the Stokes-Einstein equation<sup>[32]</sup>.

$$D = \frac{k_B T}{6\pi \eta r}$$

D= diffusion constant

$k_B$  =Boltzmann's constant

T= absolute temperature

$\eta$  = viscosity

r = radius of the spherical particles

The viscosity of the ionic liquids can be related to the cations and anions used. The alkyl group on the imidazolium cations can increase the viscosity of the ionic liquid as the chain gets longer. This is due to the increase in van der Waals forces<sup>[33]</sup>. Viscosity of the RTILs also changes as the size, shape, and molar mass of the anion used changes. As the anion becomes smaller, and more symmetric, the RTILs become more viscous<sup>[33, 34]</sup>. A symmetrical anion such as  $[\text{PF}_6]^-$  and  $[\text{BF}_4]^-$  have a viscosity of 371 ( $[\text{PF}_6]^-$ ) and 112 ( $[\text{BF}_4]^-$ ) mPa\*s (Pa\*s= Pascal-second), while the viscosity of a less symmetrical anion  $[\text{NTf}_2]^-$  decreases to 34mPa\*s<sup>[35-37]</sup>. From the data, one can also observe that increasing the number of fluorine atoms to the imide anion also increases the viscosity of the RTILs due to the increase in van der Waals forces<sup>[33]</sup>. The data also show that these RTILs are highly temperature dependent with a 20% change in viscosity over 5K around

room temperature<sup>[38]</sup>. Viscosities of 23 different RTILs have been reported by Okoturo and VanderNoot<sup>[36]</sup> over the temperature range from 283 to 343K, and found that most of the ionic liquids with symmetric cations fit into an Arrhenius equation while cations with functional groups fit the Vogel-Tammann-Fulcher (VTF) plot equation shown below better.

$$\sigma(T) = A T^{-1/2} \exp[-E/R(T-T_0)]$$

Where  $\sigma$  is viscosity and  $A$  is the pre-exponential factor proportional to  $T^{-1/2}$ , where  $T$  is the temperature of the RTILs is being examined.  $T_0$  is the temperature at which the transport function ceases to exist. The VTF equation describes the temperature dependence of amorphous materials such as glasses and melts. If the temperature is significantly lower than the glass transition temperature, then the equation simplified to an Arrhenius type equation. It is known that in a solvent, when the ion transport is governed by the mobility of the solvent molecules, the conductivity is depending on the free volume of the solvent<sup>[39]</sup>. Although RTILs do not require the addition of electrolyte, the conductivity of a 100% ionic liquid should be depends on the mobility of the ions exist in it. Thus, the viscosity is an important factor that will influence the conductivity of the RTILs<sup>[40]</sup>. From the VTF equation, one can see that by increasing the temperature of the ionic liquid, the viscosity will decrease. As a result, the ion mobility will increase. Thus, charges can pass through the analyte easier, which in turn increase the conductivity.

Research has also been done in applications such as electrochemical capacitor<sup>[41]</sup>, catalysis in organic synthesis<sup>[42]</sup> using mixture of ionic liquid with other organic solvents. As noted that when ionic liquid is mixed with a solvent, the conductivity increases. One of the most abundant solvents that exist in the planet is water, which can be dissolved

into the ionic liquid from the atmosphere if the ionic liquid is not kept under vacuum when stored, even for the hydrophobic RTILs<sup>[43]</sup>.

When the water content in the RTIL increases, the viscosity decreases. The conductivity of the RTIL increases subsequently. This might seem like an advantage at the first glance. However, research done by Compton *et. al.* shows that even though the conductivity of the RTIL has increased, the electrochemical window of the RTIL however was narrowed<sup>[26]</sup>. The reduction of the electrochemical window was found to occur at both anodic and cathodic limits. This reduction of the electrochemical window was found due to the water electrolysis<sup>[44]</sup>. In our case, we were using ionic liquids that contained  $\text{PF}_6^-$  anion. This anion is known to go through hydrolysis when in contact with water to form hydrogen fluoride<sup>[45]</sup>.

## II. Experiments

### 2.1. Equipment

All electrochemical oxidation/reduction experiments were done in a three-electrode cell. The potential is controlled using a computer controlled Cypress System Inc., model 2R potentiostat. The electrochemical analyses were done in a glass vial incorporated with a Pine Instrument Company Ceramic Patterned Electrode (usually Pt). The ionic liquid was degassed with N<sub>2</sub> overnight before the electrochemical experiment is carried out in order to eliminate O<sub>2</sub> from interfering with the analyte and also to allowed the analyte to dissolve.

All UV-visible spectra were taken using the HP-8452A photo-diode array spectrometer. The analyte was diluted to about 0.05 mM or less (unless otherwise noted) in order to obtain a spectrum of the Soret-band of the porphyrin. When running the spectroelectrochemistry experiments, an independent Cypress System Inc. OMNI-101 microprocessor controlled potentiostat is used. The data collected from the potentiostat was recorded using e-DAQ e-corder 401, which was triggered by a micro switch embedded in the shutter system of the UV-visible spectrometer. As the shutter is activated in the UV-visible spectrometer, the switch was triggered which completed a home-made open circuit that sent a signal to the e-recorder. The e-corder then recorded the potential as well as the current from the potentiostat.

The temperature of the UV-visible sample was controlled by a Quantum Northwest temperature controller. If the experiment that was done at a temperature other

than the standard room temperature, the sample holder in the UV-visible spectrometer was replaced by another sample holder which had a built-in heating/cooling element.

The conductivity test for the ionic liquid was carried out by using a YSI model 35 conductance meter. The resistance of the ionic liquid was measured by immersing a probe into the ionic liquid. When in the ionic liquid, the two electrodes in the probe will complete a circuit where the resistance can be measured as current is passed through the ionic liquid.

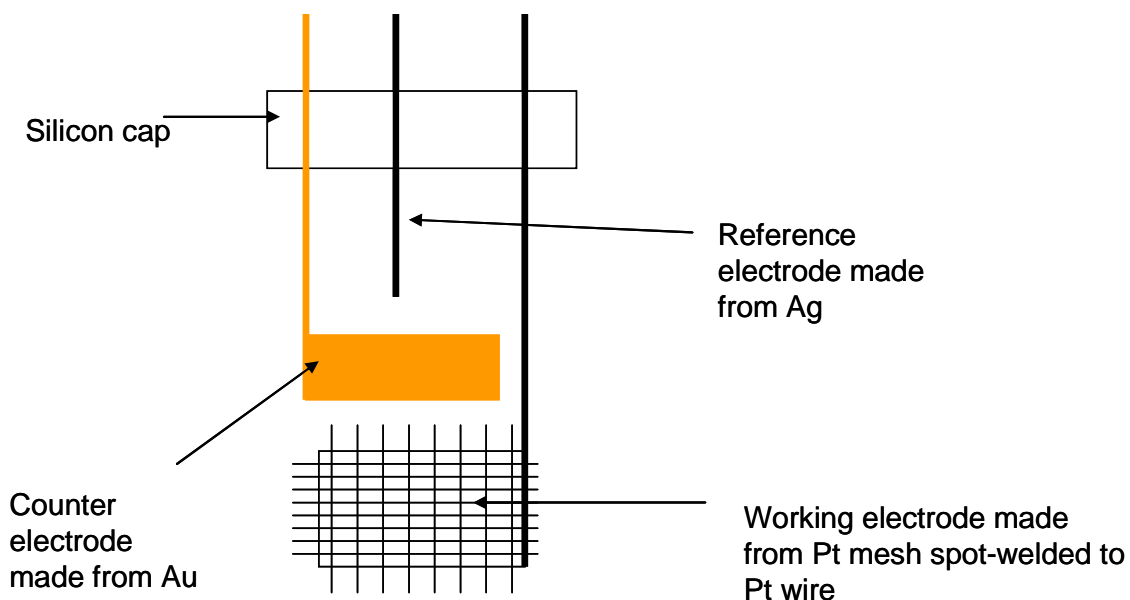


**Figure 2.1. Schematic of electrode used in a 5mm UV-visible cell.**

Above is a schematic of the design for the electrodes used in the spectroelectrochemistry experiments. The electrodes were made in a proper length in order to be fitted into a rectangular 5mm UV-visible cell, where the light path was directly passed through the Pt mesh. The solution was then filled to the point where the silver reference wire was immersed in the solution. The electrodes were passed through

the silicon cap which was cut in a way so that it could seal the UV-visible cell to minimize air from getting into the solution.

## **2.2. Materials**

The metalloporphyrins complexes Co(II)TPP (98%) and Mn(III)TPPCl (98%) were used as received from Aldrich. The Fe(III)TPPCl were obtained from Midcentury Chemical Co., and were also used as received.

Dichloromethane, spectrophotometric grade, 99.7+%, stabilized with amylene, used in the synthesis of the RTILs was used as received from Alfa Aesar without further purification.

Chloroform also used in synthesis of RTILs is purchased from Aldrich (spectrophotometric grade, 99.8%), and was used without any further purification.

## **2.3. Procedures**

### **2.3.1. Synthesis of 1-Butyl-3-methylimidazolium bromide (BMIMBr) ionic liquid**

1-Butyl-3-methylimidazolium bromides were synthesized by reaction of either using neat 1-methylimidazole (Aldrich, 99%) and 1-bromobutane (Alfa Aesar, 98+%) at 110 to 120°C in a round bottomed flask submersed in an oil bath for 2 hours; or 1-methylimidazole and 1-bromobutane in chloroform at 90°C in a round bottomed flask submersed in an oil bath for 24 hours.

Reactions of neat 1-methylimidazole and 1-bromobutane will yield almost 99% 1-butyl-3-methylimidazolium bromide without purification and can be accomplished in a shorter time<sup>[46]</sup>. A round bottom flask with 1:1.3 equivalent molar amount of 1-

methylimidazole and 1-bromobutane was heated to 120 to 140°C in a oil bath for 20 to 30 minutes. An emulsion process will take place during the heating. As the emulsion disappears, the liquid will turn into a transparent golden color which is slightly viscous. The oil bath is removed and allows the mixture is allowed to cool while being stirred for another 20 to 30 minutes. The solution is then heated to 120 to 140°C for another hour. At the end of the heating, the temperature is reduced to 100 to 120°C and the mixture is dried under vacuum for a period of 24 hours or longer in order to remove excess starting materials (mainly bromobutane).

Proton  $^1\text{H}$ -NMR spectra were obtained using the Varian 300MHz in order to determine the purity of the ionic liquid made. The results gathered were compared to the results found in literature<sup>[46]</sup>. Figure 2.2 is the proton  $^1\text{H}$ -NMR spectra of BMIMBr collected using chloroform-*d* as the solvent. The peaks positions were close to the reported data shown in Table 2.1 from the literature.

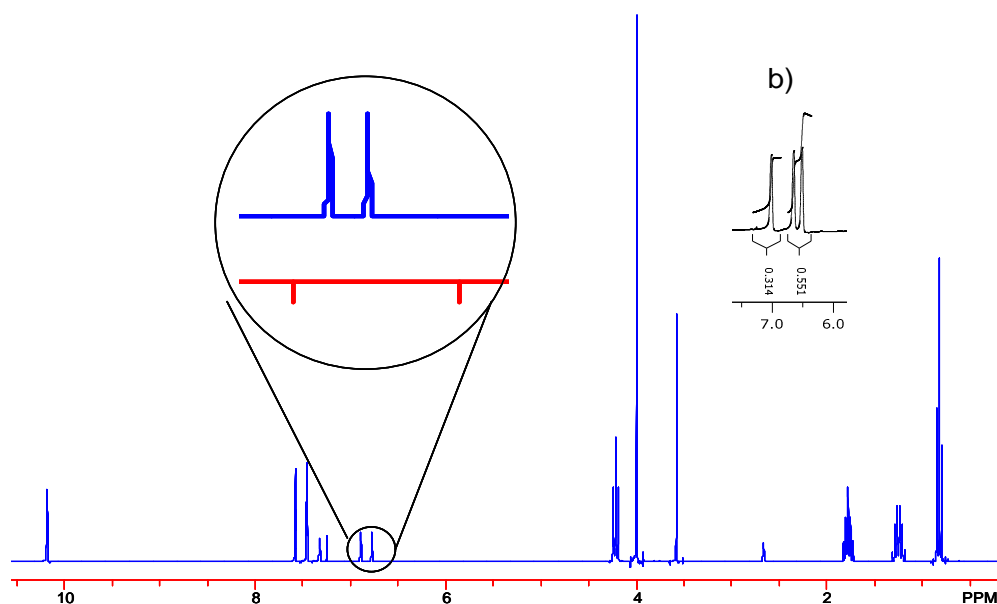


**Figure 2.2.**  $^1\text{H}$ -NMR of BMIMBr collected using chloroform-*d* as solvent, b)  $^1\text{H}$ -NMR of 1-butyl-3-methylimidazole.



**Table 2.1. Proton chemical shifts for BMIMBr from literature<sup>[46]</sup>.**

Compound	CH <sub>3</sub> N	NCHN	NCHCHN	NCHCHN	NCH <sub>2</sub>	NCH <sub>2</sub> CH <sub>2</sub>	alkyl	Term. CH <sub>3</sub>
<b>4</b>	4.15 (s)	10.30 (s)	7.80 (t, 1.7)	7.65 (t, 1.7)	4.36 (t, 7.3)	1.97 (m)	1.34 (4H, m)	0.89 (t, 6.7)

From Figure 2.2, there is some trace of un-reacted 1-methylimidazole existed in the solution which can be seen from 6.8 to 7.4 ppm. This explained why the yield obtained by us is only roughly 75 to 80% instead of 89% as reported in literature.

### **2.3.2. Synthesis of 1-Butyl-3-methylimidazolium hexafluorophosphate (BMIMPF<sub>6</sub>) ionic liquid**

1-Butyl-3-methylimidazolium hexafluorophosphate was synthesized by using 1-butyl-3-methylimidazolium bromide as a precursor<sup>[47]</sup>. In a round bottom flask, equal molar amounts of 1-butyl-3-methylimidazolium bromide (usually about 0.37 mol) and potassium hexafluorophosphate (0.37 mol, Alfa Aesar, 99% min) were dissolved in distilled water. The mixture of solution was then stirred at room temperature for at least 2 hours. The result was a two phase system. The organic phase was washed with excess amount of water (at least 5 X 100 mL). The ionic liquid was then dried under vacuum for about 24 hours. After the ionic liquid was removed from the vacuum, 35 g of anhydrous magnesium sulfate and 100 mL of dichloromethane were added. After one hour, the suspension was then filtered. The ionic liquid was then put under a vacuum at about 50°C for about 24 hours in order to remove any volatile material. The result was a yellowish viscous liquid of 1-butyl-3-methylimidazolium hexafluorophosphate.

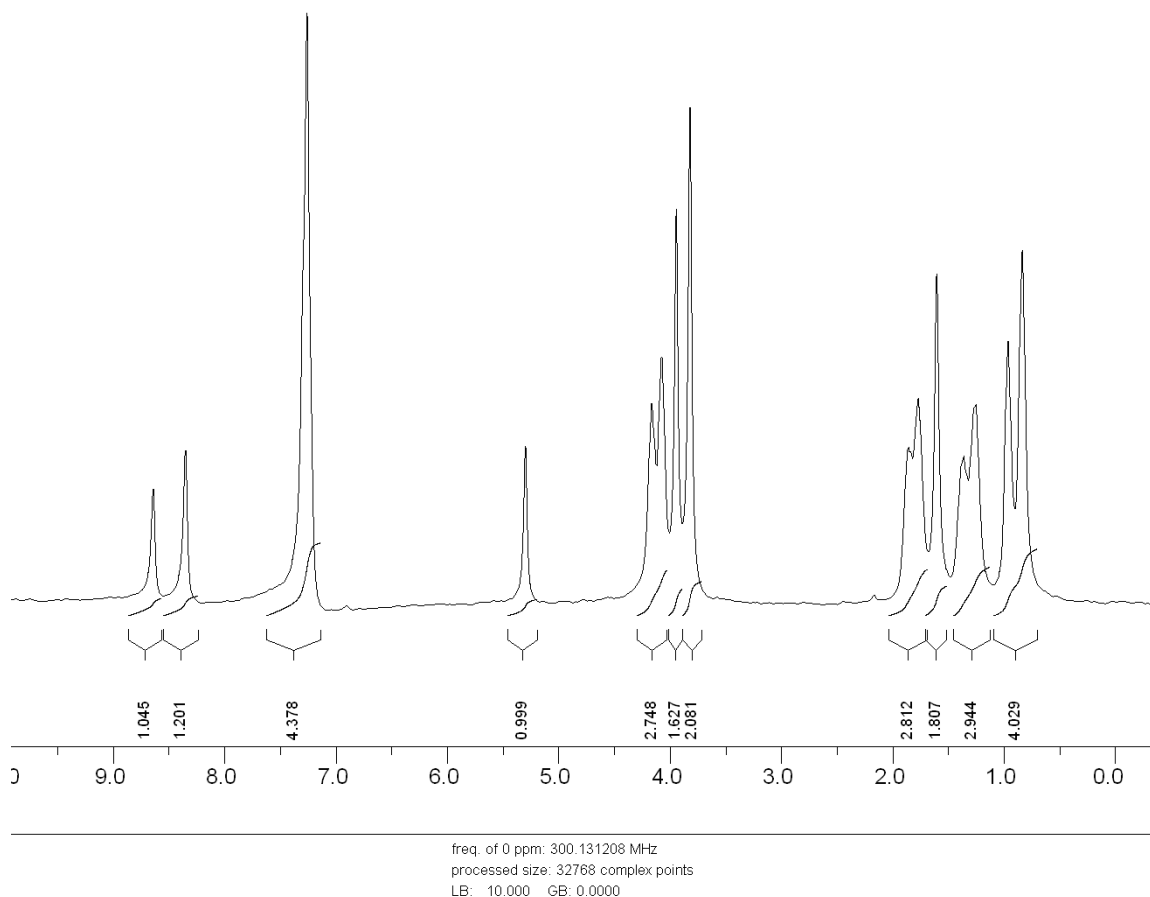


**Figure 2.3**  $^1\text{H-NMR}$  of  $\text{BMIMPF}_6$  collected using chloroform-*d* as solvent.

Figure 2.3 above is the proton  $^1\text{H-NMR}$  spectra of  $\text{BMIMPF}_6$  collected using chloroform-*d* as the solvent. The  $\text{BMIMPF}_6$  synthesized was found to be relatively clean as there is no trace of any starting material shows up in the proton NMR. The  $^1\text{H-NMR}$  peaks are found to be close to as reported in literature appear as follows:  $\delta$  0.72 (t), 1.15 (sextet), 1.68 (qnt), 2.25 (s, br), 3.73 (s), 4.05 (t), 7.22 (s), 7.30 (s) and 8.26 (s)<sup>[48]</sup>. However, again the yield obtained by us (65%) is slightly lower than reported in literature (71%) from the starting materials.

### III. Results And Discussion

#### 3.1. UV-visible studies of metalloporphyrins in ionic liquid

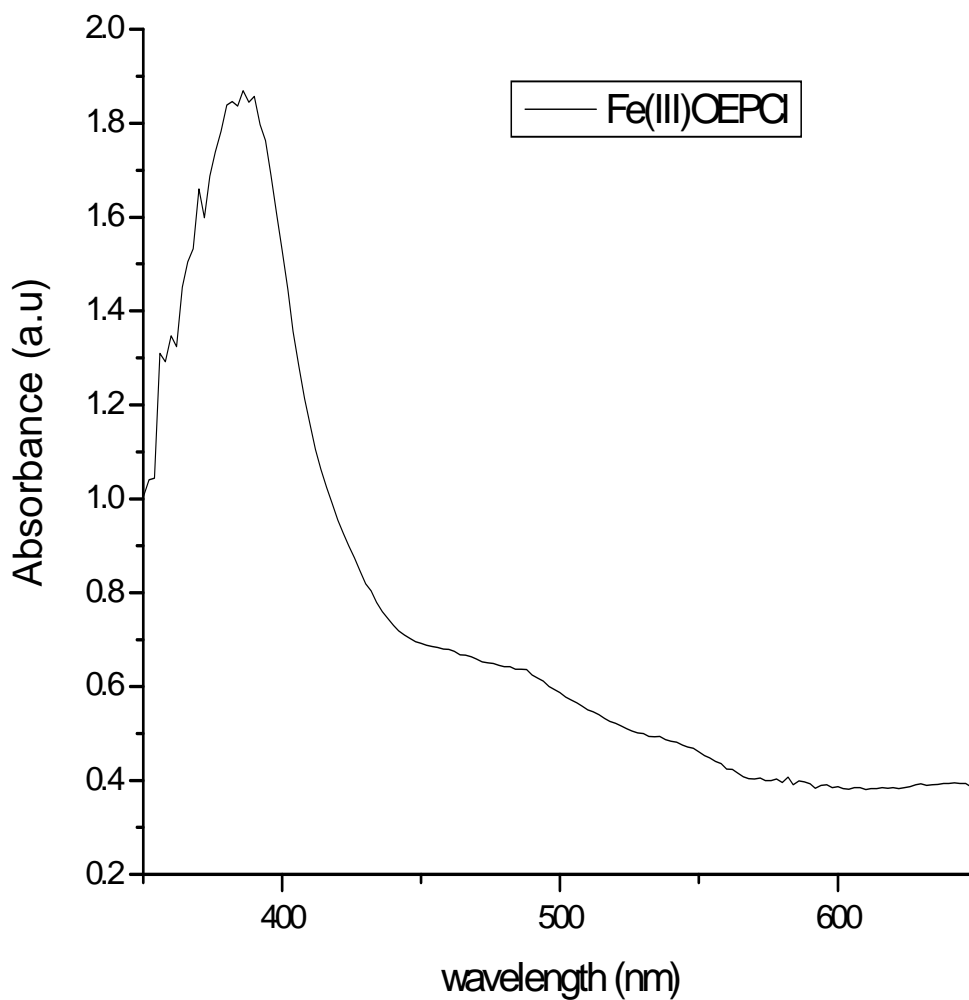
All UV-visible spectra were collected using the HP-8452A diode array spectrometer as mentioned in Chapter 2. Ionic liquid (either BMIMBr or BMIMPF<sub>6</sub>) was used as background spectra. The concentration of the metalloporphyrin was adjusted to 0.02 to 0.03 mM in order to acquire an UV-visible spectrum without the Soret band being saturated.

The purpose of acquiring UV-visible spectra was to confirm that the metalloporphyrins and the ionic liquid did not react with each other when added. This step was particularly crucial because when one incorporates UV-visible with CV together, one can determine if the changes in the UV-visible spectra only occur due to electrons added to the metalloporphyrin system. Since the metalloporphyrin added into the IL was very small (0.02mM in 5mL solution), the metalloporphyrin dissolved easily. However, at larger concentration for electrochemical experiments, dissolving the metalloporphyrin in IL was a problem. This will be discussed later in Section 3.2. The UV-visible spectra obtained were similar to those collected in chloroform or CH<sub>2</sub>Cl<sub>2</sub>.

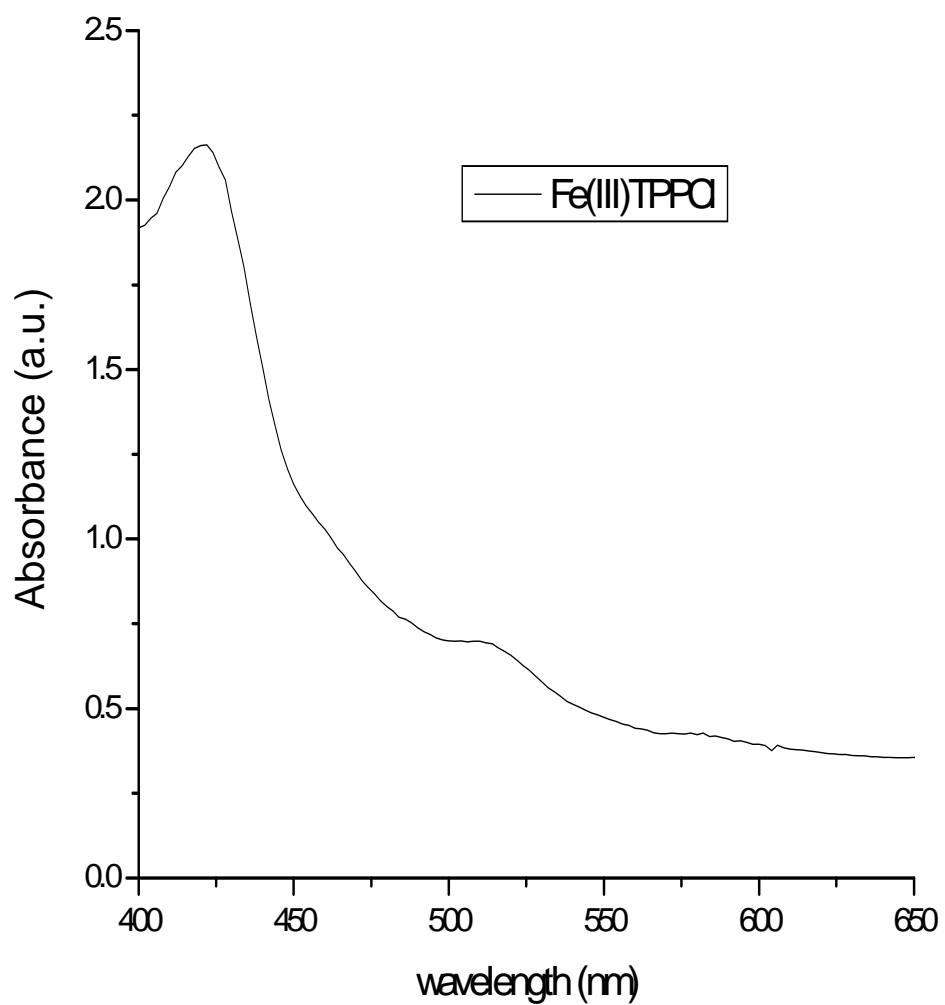
Figure 3.1a and d are the UV-visible spectra of Fe(III)OEPCl in BMIMBr and in BMIMPF<sub>6</sub>. The Soret band and Q bands are similar to the one collected using CH<sub>2</sub>Cl<sub>2</sub> as solvent<sup>[49]</sup>.

Figure 3.1b and 3.1e are the UV-visible spectra of Fe(III)TPPCl in BMIMBr and BMIMPF<sub>6</sub>. Both spectra collected are consistent with the spectra shown in chapter 1(Figure 1.5), which was collected using CHCl<sub>3</sub> as solvent.

Figure 3.1c and 3.1f are the UV-visible spectra of Mn(III)OEPCI in BMIMBr and BMIMPF<sub>6</sub>. The Soret band at around 440 nm is sharper compared to the iron porphyrins which is consistent to the one reported in literature<sup>[50]</sup>.



**Figure 3.1a.** UV-visible spectrum of Fe(III)OEPCI in BMIMBr.



**Figure 3.1b.** UV-visible spectrum of Fe(III)TPPCl in BMIMBr.

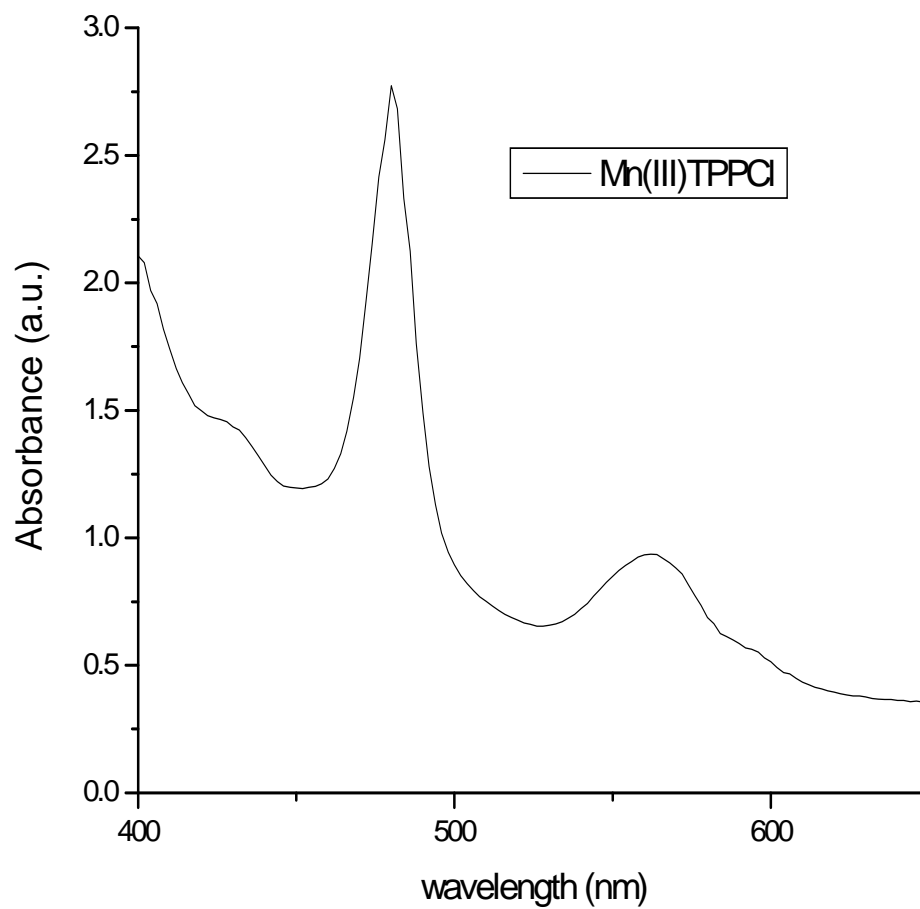


**Figure 3.1c. UV-visible spectrum of Mn(III)TPPCl in BMIMBr.**

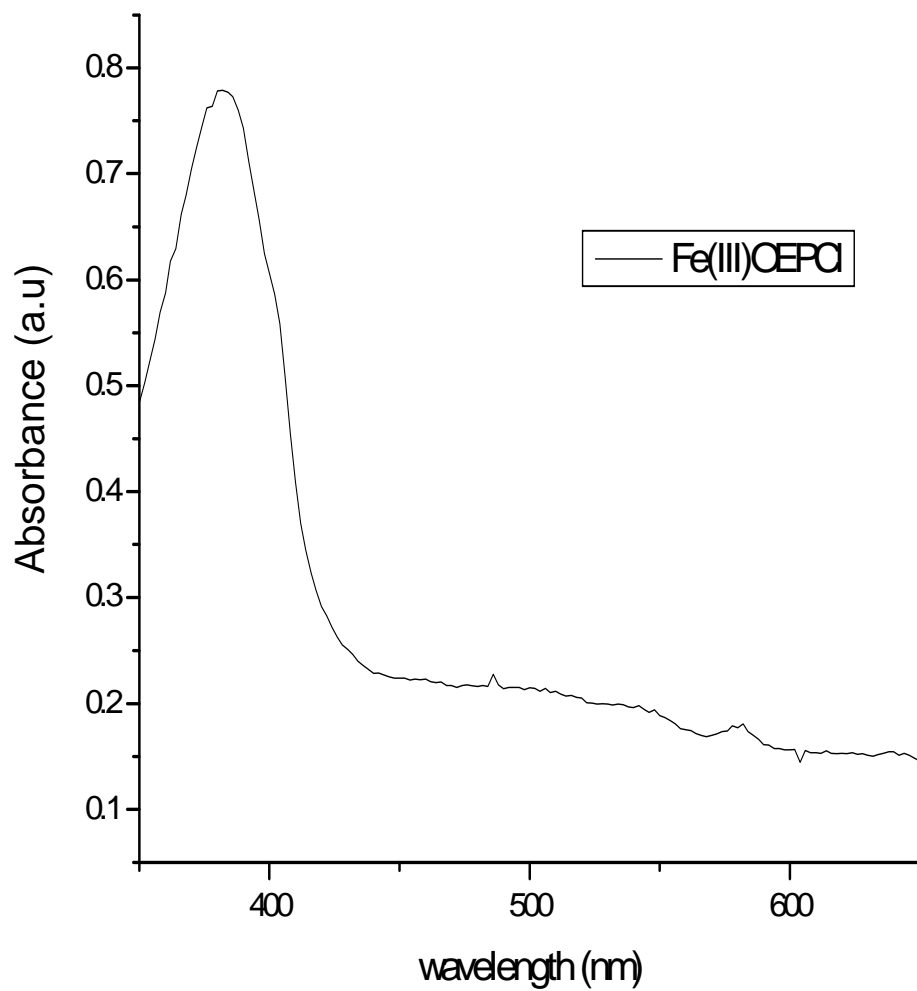


**Figure 3.1d.** UV-visible spectrum of Fe(III)OEPCI in BMIMPF<sub>6</sub>.

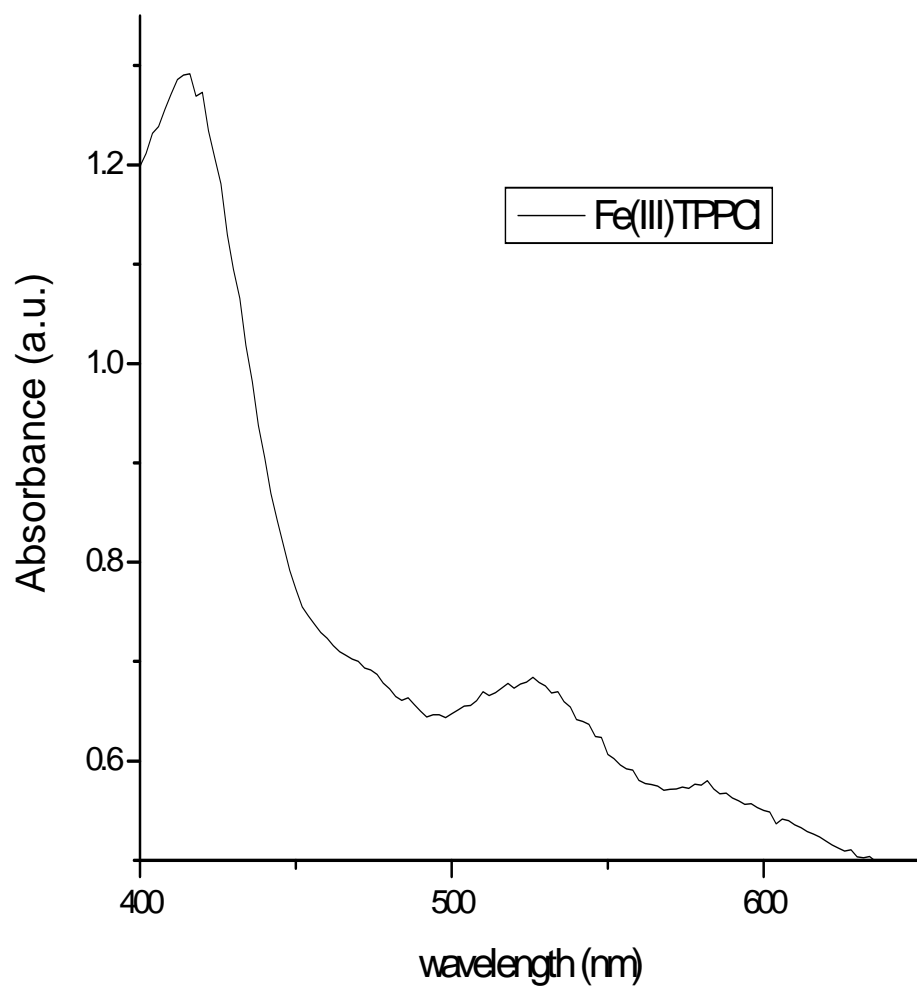


**Figure 3.1e. UV-visible spectrum of Fe(III)TPPCl in BMIMPF<sub>6</sub>.**



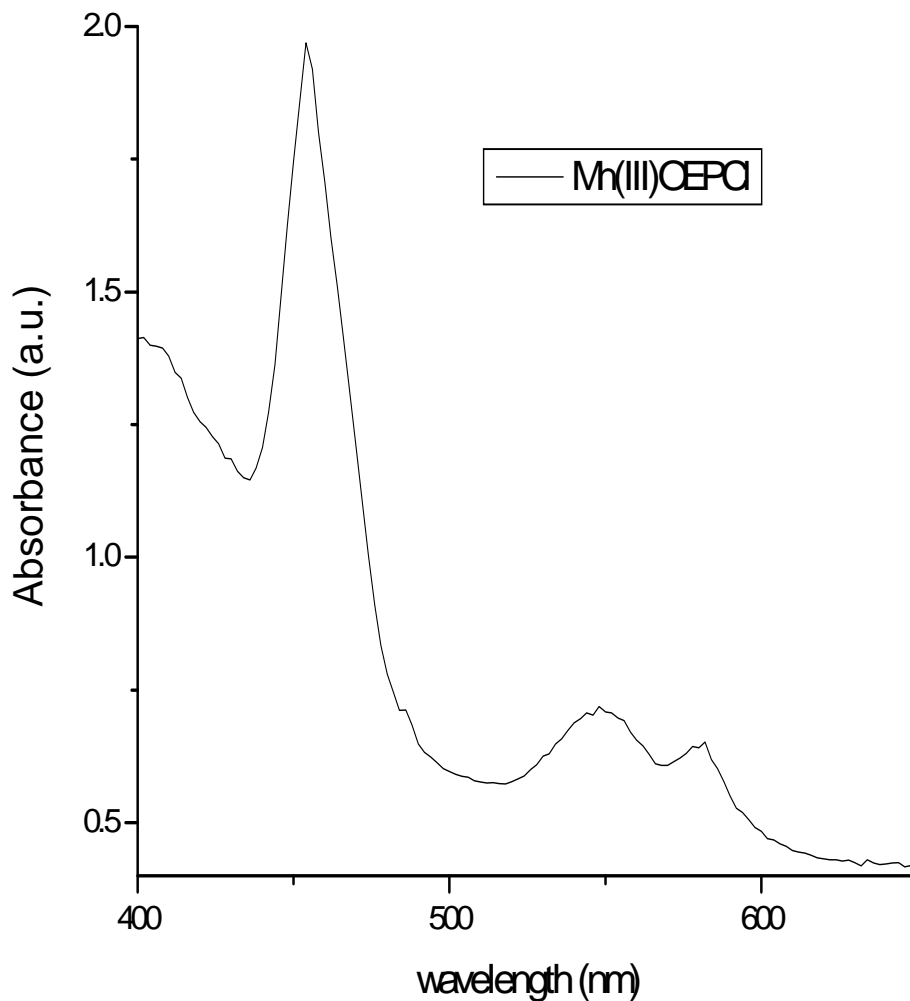


**Figure 3.1f. UV-visible spectrum of Mn(III)OEPCl in BMIMPF<sub>6</sub>.**

### **3.2. Cyclic Voltammogram (CV) of metalloporphyrins in ionic liquid**

Figure 3.2a-d show the cyclic voltammograms for the first reduction of Fe(III)OEPCl, Fe(III)TPPCl, Mn(III)OEPCl and ferrocene with BMIMBr as the solvent.

From the Figure 3.2a, the reduction potential of the wave suggests that the reduction reaction is independent of the porphyrin ring as it was due to the reduction of  $\text{Fe}^{3+} + \text{e}^- \rightarrow \text{Fe}^{2+}$ . The figure also showed that the reduction wave was irreversible at

lower scan rates. This Fe(III)TPPCl (Figure 3.2b) also showed similar behavior of irreversibility for the first reduction wave at scan rates lower than 100mV/s. However, as the scan rate increased, the reversibility of the first reduction wave improved. This indicated that the reduction product may undergo a slow chemical reaction. A possible chemical reaction that could be happening was the exchange of the ligand. Because of the large excess of Br<sup>-</sup> ligand and the fast ligand exchange, the axial ligand was probably bromide in the ferric complex.

Comparing the reduction potential of Fe(III)OEPCl and Fe(III)TPPCl, the Fe(III)TPPCl has a less negative potential. This is not so surprising because the Fe(III)TPPCl has four electrons-withdrawing substituent rings attach to it. Surprisingly, the potential difference is very small (~35mV). As reported by Kadish<sup>[51]</sup> in a paper in 1973, the Fe<sup>3+</sup> ⇌ Fe<sup>2+</sup> transition occurs at -0.24V for Fe(III)OEP(OH) which is quite similar to our results. In the same paper, Kadish also reported the Mn<sup>3+</sup> ⇌ Mn<sup>2+</sup> transition occurs at -0.42V which is very close to the value obtained by us (-0.49V shown in Figure 3.2c). However, since the reference electrodes used in both cases are different, it is normal that the electrode potentials are slightly different.

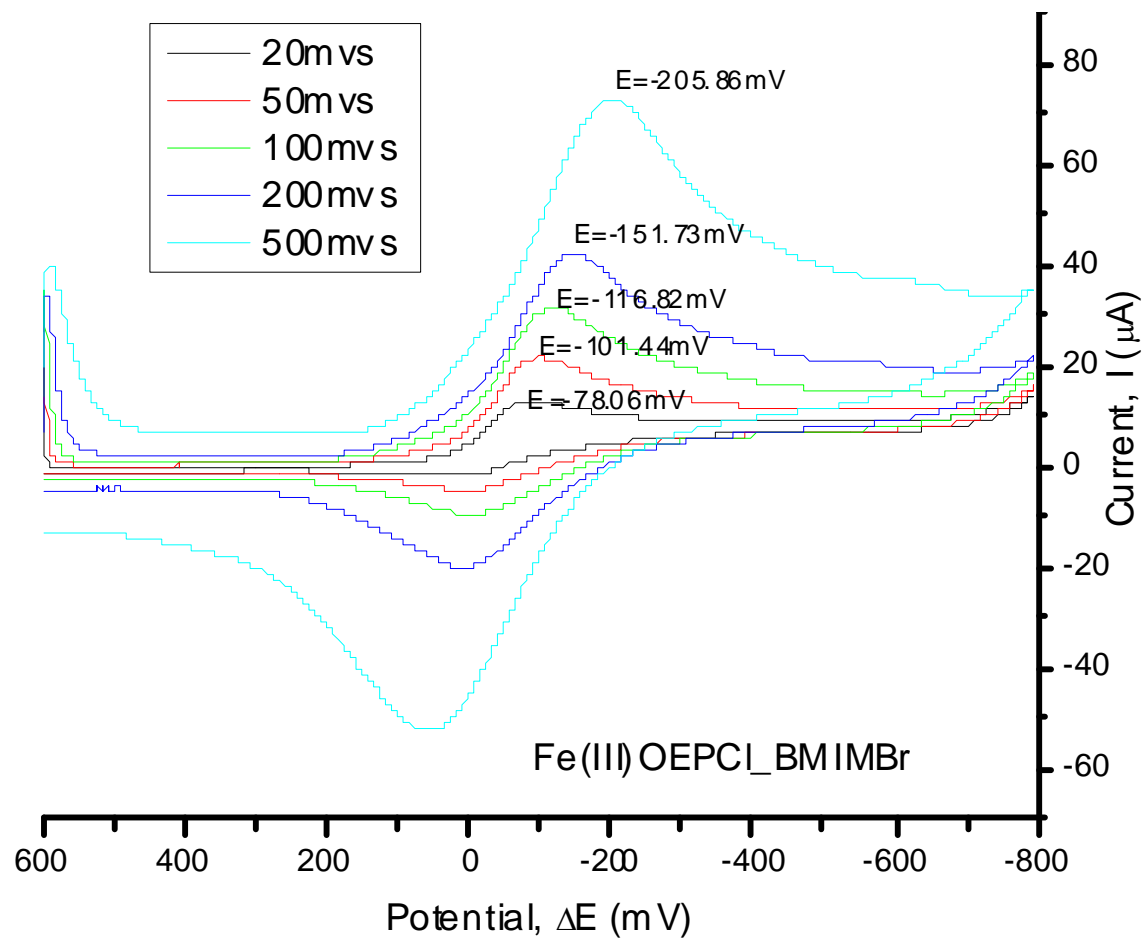


Figure 3.2a. CV of Fe(III)OEPCl in BMIMBr.

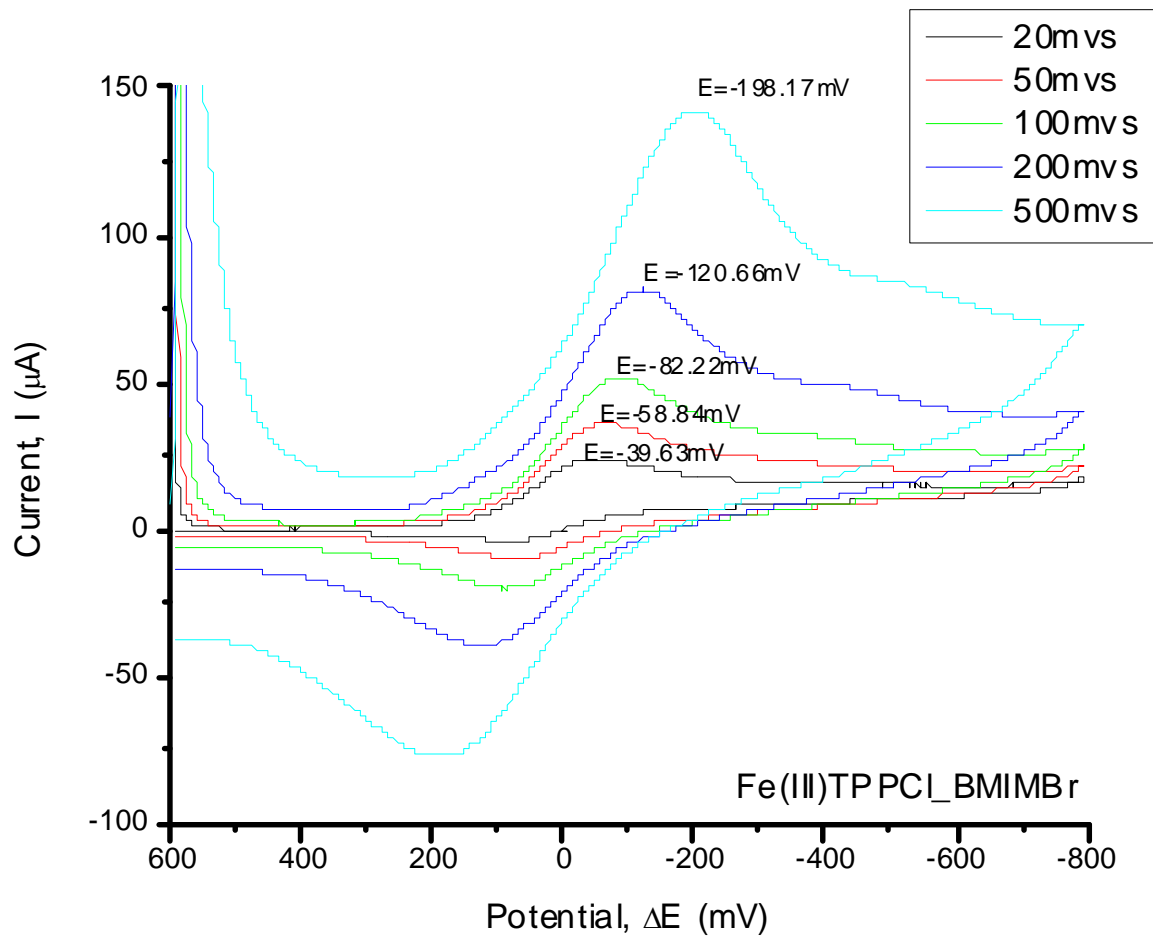
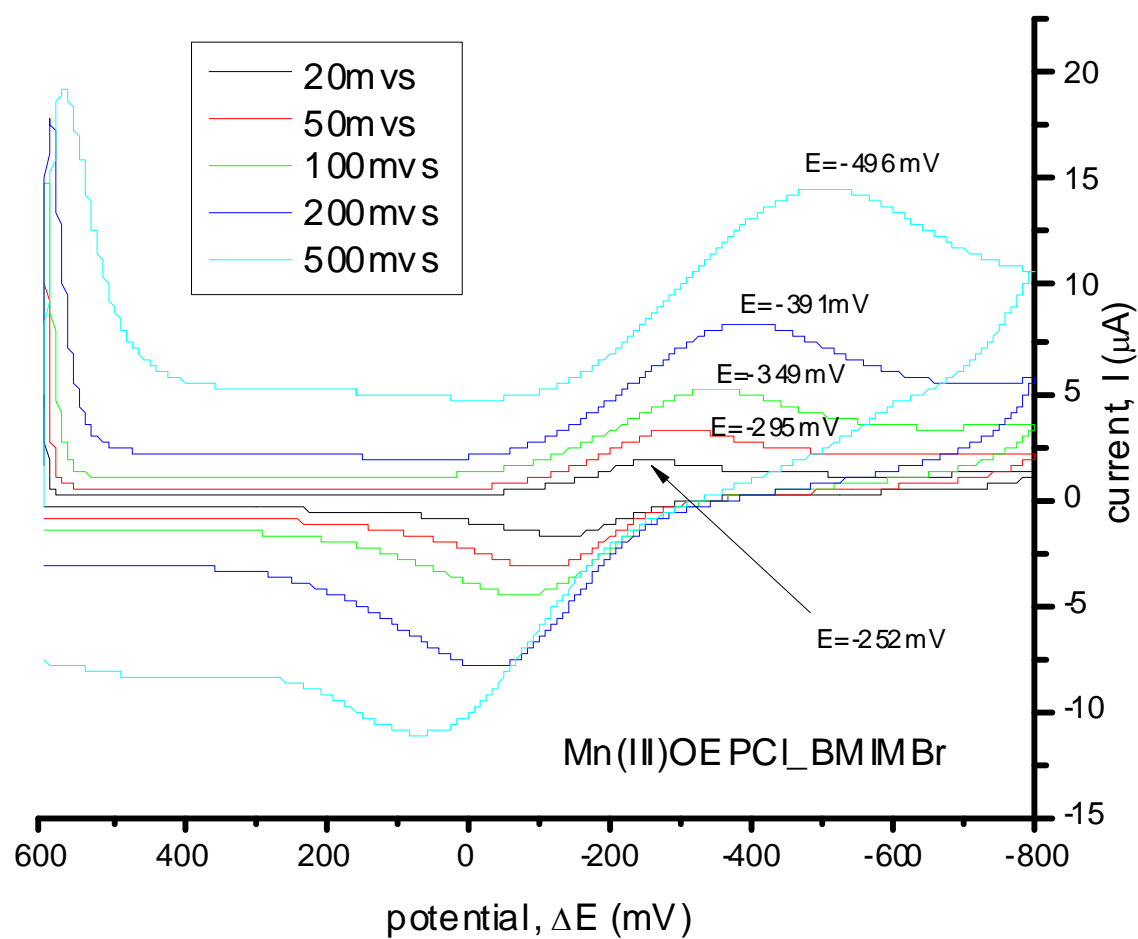


Figure 3.2b. CV of Fe(III)TPPCL in BMIMBr.



**Figure 3.2c. CV of Mn(III)OEPCI in BMIMBr.**

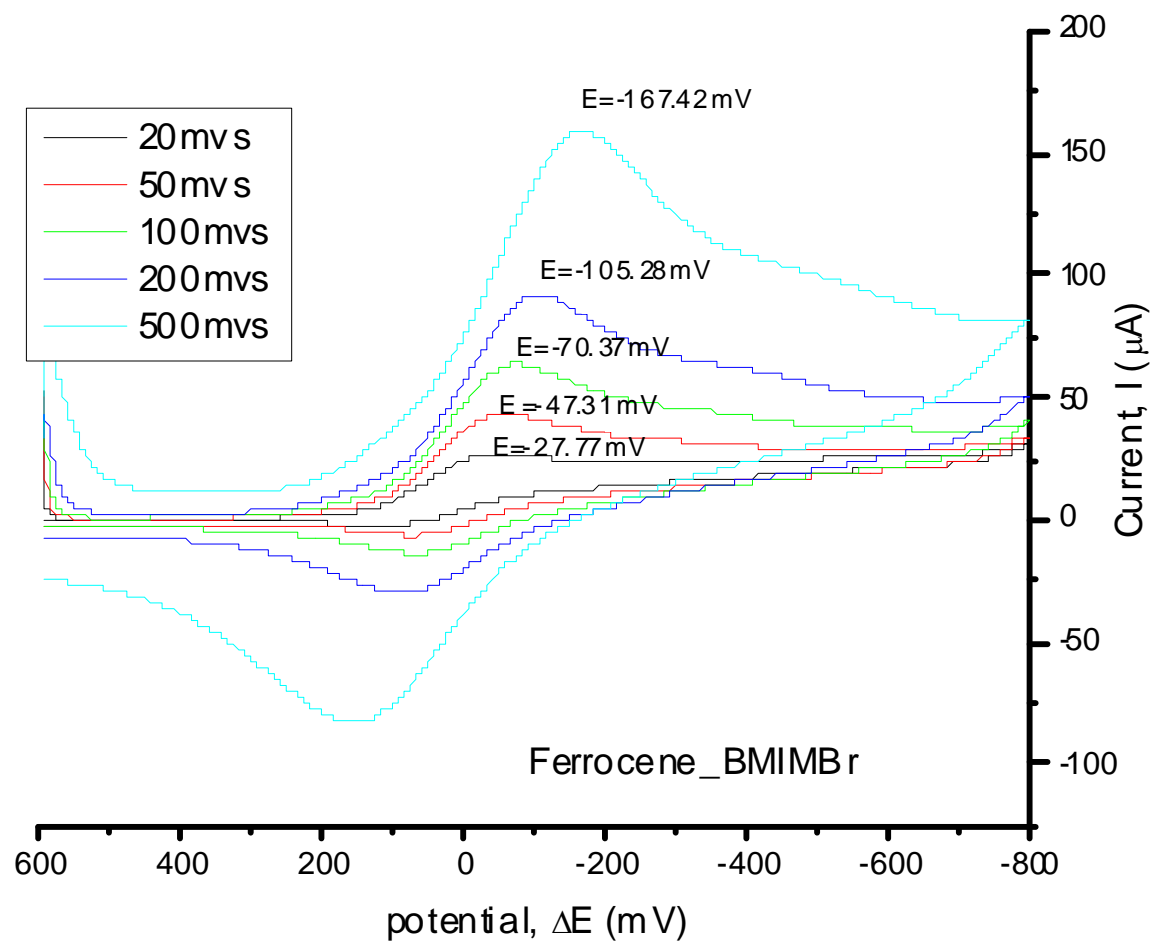


Figure 3.2d. CV of Ferrocene in BMIMBr.

**Table 3.1a. Electrochemical data from the CV of 8mM Fe(III)OEPCL in BMIMPF<sub>6</sub>.**

<i>Scan rate (mV/s)</i>	$I_{p,f}$	$E_{p,f}$	$E_{p,r}$	$I_p/v^{1/2}C$	$(E_{p,f}+E_{p,r})/2$
20	12	-78	-50	0.106	-64
50	21	-101	-35	0.1174	-68
100	31	-117	-30	0.1225	-74
200	42	-152	-5	0.1174	-79
500	72	-206	46	0.1273	-80

**Table 3.1b. Electrochemical data from the CV of 8mM Fe(III)TPPCL in BMIMPF<sub>6</sub>.**

<i>Scan rate (mV/s)</i>	$I_{p,f}$	$E_{p,f}$	$E_{p,r}$	$I_p/v^{1/2}C$	$(E_{p,f}+E_{p,r})/2$
20	20	-40	53	0.1758	7
50	35	-59	60	0.1957	01
100	52	-82	81	0.2056	-1
200	77	-121	117	0.2152	-2
500	137	-198	195	0.2422	-2

**Table 3.1c. Electrochemical data from the CV of 1mM Mn(III)OEPCL in BMIMPF<sub>6</sub>.**

<i>Scan rate (mV/s)</i>	$I_{p,f}$	$E_{p,f}$	$E_{p,r}$	$I_p/v^{1/2}C$	$(E_{p,f}+E_{p,r})/2$
20	1.7	-252	-126	0.1202	-189
50	3	-295	-100	0.1342	-198
100	4.9	-349	-90	0.1575	-220
200	8	-391	-22	0.1789	-207
500	15	-496	76	0.2121	-210

**Table 3.1d. Electrochemical data from the CV of 8mM Ferrocene in BMIMPF<sub>6</sub>.**

<i>Scan rate (mV/s)</i>	$I_{p,f}$	$E_{p,f}$	$E_{p,r}$	$I_p/v^{1/2}C$	$(E_{p,f}+E_{p,r})/2$
20	25	-28	24	0.221	-2
50	45	-47	49	0.2516	1
100	63	-70	72	0.2490	1
200	88	-105	98	0.2460	-3
500	158	-167	162	0.2793	-3

Table 3.1a-d is the summary of the CV of metalloporphyrins from Figure 3.2a-d. By calculating the  $I_p/v^{1/2}C$ , one can compare to a known system to find out how many electrons are being transfer from the electrode to the analyte in the reaction. A good example to use as comparison is the ferrocene/ferrocenium redox reaction since the redox reaction only involved one electron. Comparing the data from Table 3.1, we observed

that the reduction reaction of the metalloporphyrins involved less than one electron if compare to ferrocene/ferrocenium. The reason this phenomenon is observed is due to the solubility problem of the metalloporphyrins in pure RTILs. During the sample preparation, we noted that Fe(III)TPPCl dissolved in RTILs easier than Fe(III)OEPCl and Mn(III)OEPCl. As we can see, the data in Table 3.1c shows that the  $I_p/v^{1/2}C$  value is close to the one in ferrocene/ferrocenium.

Compton *et. al.* reports the voltammetric characterization of ferrocene/ferrocenium redox couple in RTILs<sup>[32]</sup>. The  $E_{1/2}$  value for the one electron oxidation of ferrocene/ferrocenium is found to be at +385mV vs. Ag (at 1000 mV/s). The  $E_{1/2}$  value collected by us is at close to zero potential using a 0.5 mm diameter silver wire as reference. The difference could be cause by a numbers of things. In the literature it was reported that the authors used a micro electrode where we were using a macro electrode. The RTIL used in the literature is 1-butyl-3-methylimidazolium bis(trifluoromethylsulfonyl)imide (BMIMNTf<sub>2</sub>), where we were using BMIMBr.

Comparing the  $E_{1/2}$  of the metal reduction in the metalloporphyrins with those done in conventional solvent with supporting electrolyte added, the difference is quite consistent for the Fe(III)/Fe(II) and Mn(III)/Mn(II). Reported by Kadish *et. al.*, the redox potential for Fe(III)/Fe(II) done in 0.01 M TBAP in DMSO is found to be at -240mV vs SCE<sup>[51]</sup>. The difference between ours and the one in literature is about 200mV. The authors also reported the redox potentials of Mn(III)/Mn(II) done in the same solvent to be at -420mV vs SCE. The difference between ours and the literature is also about 200mV.



Since we were unable to use ferrocene/ferrocenium redox potential to standardize the reduction potential of the metalloporphyrins, we have to rely on the spectral changes in spectroelectrochemical experiments in order to observe the reduction process.

### **3.3. Studies done by incorporating CV with UV-visible of metalloporphyrins in ionic liquid**

While the CV was able to identify at what potential metalloporphyrins can accept or release an electron into the system, it was unable to give us any information as to where the electron transfer had taken place. However, when one performs the CV along side with the UV-visible, one can also at the same time obtain spectroscopic information which could lead to the determination of the structure of the metalloporphyrin. The changes will allow us to understand if the metal or the porphyrin ring was reduced. From previous CV data, we can gather the information at what potential the metalloporphyrin was reduced. Hence around that potential region, we can determine which part of the metalloporphyrin is being reduced with the help of the UV-visible spectra.

Due to the limitation of the UV-visible spectrometer, the concentrations of the metalloporphyrins in the ionic liquid had to be reduced in order to obtain useable spectra in a 5mm UV-visible cell capable of running CV at the same time. The cell design was previously described in Chapter 2.

#### **3.3.1. Studies done on Co(II)TPP in ionic liquid**

##### **3.3.1.1. Reason Co(II)TPP is used in our case**

The reason Co(II)TPP was used in the investigation is due to the fact that

Co(II)TPP is easily oxidized to Co(III)TPP, then to Co(III)TPP<sup>+</sup>. However, the CV collected by us only shows only one single oxidation peak at around +1700mV. When UV-visible spectra were collected at the same time, the changes observed were minimal. The Soret band at 434nm decreased a little, while the shoulder at 410nm became more distinct. As predicted, there should be more significant changes in the UV-visible spectrum as Co(II)TPP oxidized to Co(III)TPP, since there was a change in its coordination environment (i.e. square planar or square pyramidal for Co(II)TPP and Co(III)TPP respectively).

After numerous experiments, we found that the conductivity of the RTIL was not sufficient to carry the current needed in the spectroelectrochemistry. In order to increase the conductivity of the RTIL, tetrabutylammonium perchlorate (TBAP) was added into the solution. The results obtained will be discussed in Section 3.3.1.2.

### **3.3.1.2. What happens when electrolyte is added into the ionic liquid**

Various concentrations of TBAP (0.1M, 0.05M, 0.01M and 0.005M) were added into the RTIL along with the Co(II)TPP. The solutions were then being degassed under N<sub>2</sub> overnight in order to eliminate O<sub>2</sub> from the solutions.

Shown in Figure 3.3 is the CV of 0.1mM Co(II)TPP in 30% BMIMPF<sub>6</sub> and 70% CH<sub>2</sub>Cl<sub>2</sub>. All CVs are scanned at 100mV/s. The reason that the sample was prepared with a combination of RTIL and CH<sub>2</sub>Cl<sub>2</sub> was to decrease the viscosity of the solvent, hence increasing the mobility of the ions in it. From the figure below, one phenomenon that can be observed is that the shifting of the ring oxidation peak of the porphyrin. Similar patterns can be also being observed more clearly when different percentages of

RTIL exist in the solvent which will be discussed in Section 3.4.3. When 0.1M TBAP is added to the solution, we observed the ring oxidation peak at around 1300mV, which is close to those reported in literature<sup>[52]</sup>. However, when less electrolytes were added into the system, the oxidation peak shifted to higher potential. This makes sense because more electrolyte added to a system, it helps to eliminate the contribution of migration to the mass transfer of the electro-active species. As the concentration of electrolyte decreases, the solution resistance increases, hence, the uncompensated resistance also increased between the working and reference electrodes. As a result, by using RTILs as solvent/electrolyte, one should be able to eliminate or minimized the resistance in the system. However, as mentioned in Section 1.3.1, if using the pure RTIL, we have the problem where the solution is too viscous that it reduces the ion mobility of the porphyrins. As a result, we used a mixture of RTIL and CH<sub>2</sub>Cl<sub>2</sub>. By using the mixture, the ion mobility increases while eliminating the added electrolyte.

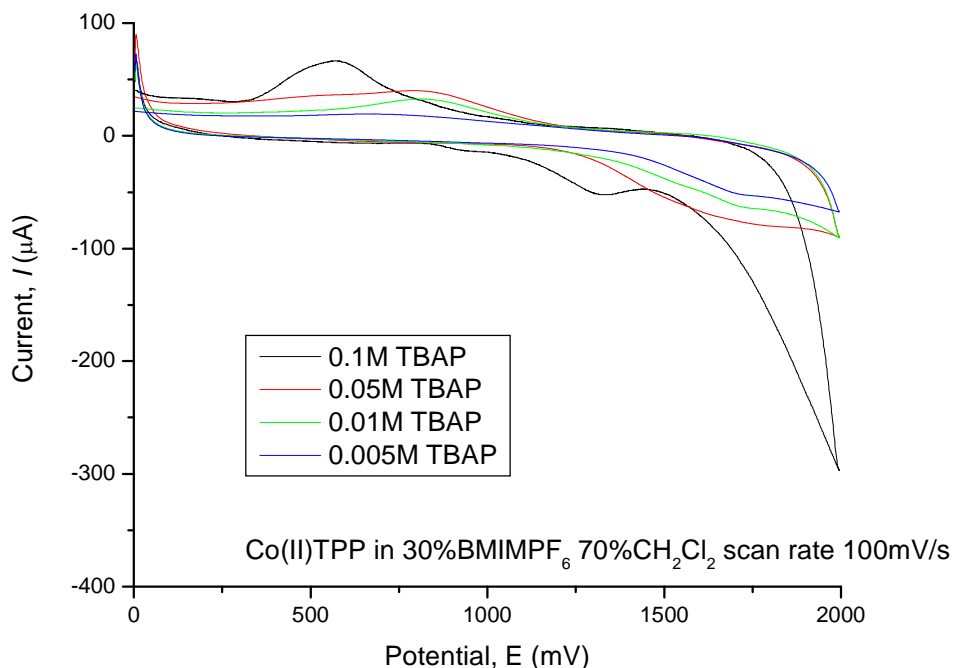


**Figure 3.3. CV of 0.1mM Co(II)TPP in 30% BMIMPF<sub>6</sub> and 70% CH<sub>2</sub>Cl<sub>2</sub>.**

### 3.3.1.3. Mixtures of different percentage of Dichloromethane added into ionic liquid as solvent

Figure 3.4 shows the CV of 0.2mM Co(II)TPP in various mixtures of CH<sub>2</sub>Cl<sub>2</sub> and BMIMPF<sub>6</sub>. All CV's are prepared at a scan rate of 100mV/s. As predicted, when the solvent consists of 90% CH<sub>2</sub>Cl<sub>2</sub>, the ions are more mobile, hence, more current passes through the system. As the RTIL increases to 20%, one can observe that the oxidation peak of the porphyrin ring shifted from 1300mV to 1400mV. When the solvent is composed of 25% CH<sub>2</sub>Cl<sub>2</sub> and 75% BMIMPF<sub>6</sub>, the oxidation peak shows up at 1650mV. The results show that by increasing the IL to the right concentration, one can eliminate the solution resistance; hence, the uncompensated resistance drops between the working and reference electrodes. At the same time, by adding just the right amount of CH<sub>2</sub>Cl<sub>2</sub> will decrease the viscosity of the IL, allowing ions to gain enough mobility to increase

the mass transfer of the electro-active species. This information obtained is crucial to spectroelectrochemistry experiments because the experiments will be done are in a thin layer cell where the solution resistance is high and the concentration of the analyte will is low (around 0.02mM).

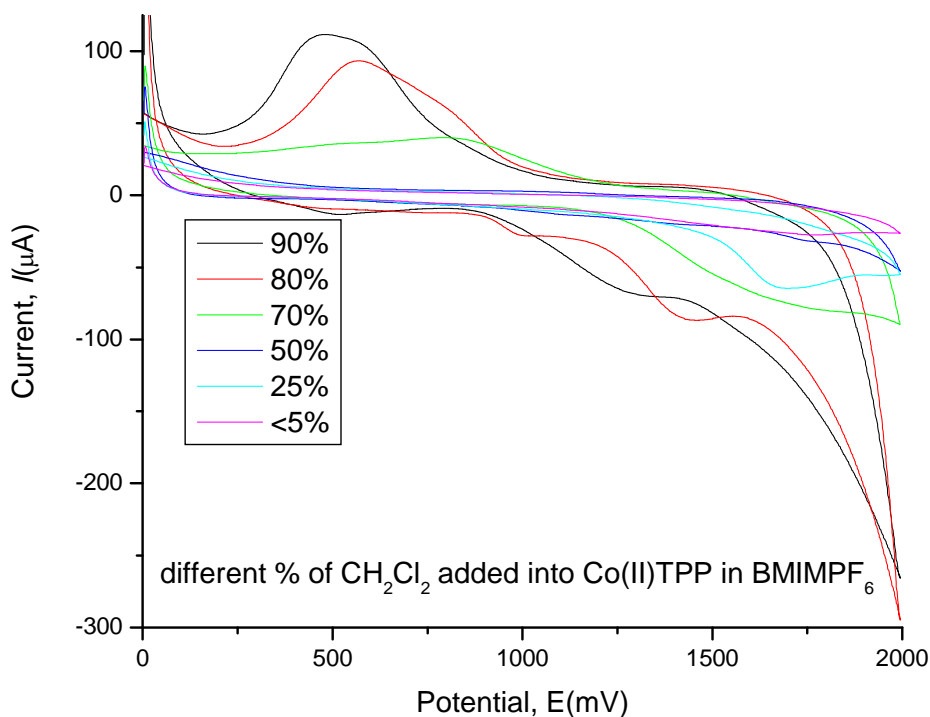


**Figure 3.4. CV of 0.2mM Co(II)TPP in various percentage of CH<sub>2</sub>Cl<sub>2</sub> in BMIMPF<sub>6</sub>.**

#### **3.3.1.4. Conductivity test done on mixture of various concentration of ionic liquid with CH<sub>2</sub>Cl<sub>2</sub>**

Conductivity is crucial to an electrochemical experiment. As mentioned earlier, most RTILs have conductivities similar to organic solvent with electrolytes added into it. Figure 3.5 shows the conductance test done on BMIMBr by varying the percentage of RTIL and CH<sub>2</sub>Cl<sub>2</sub>.

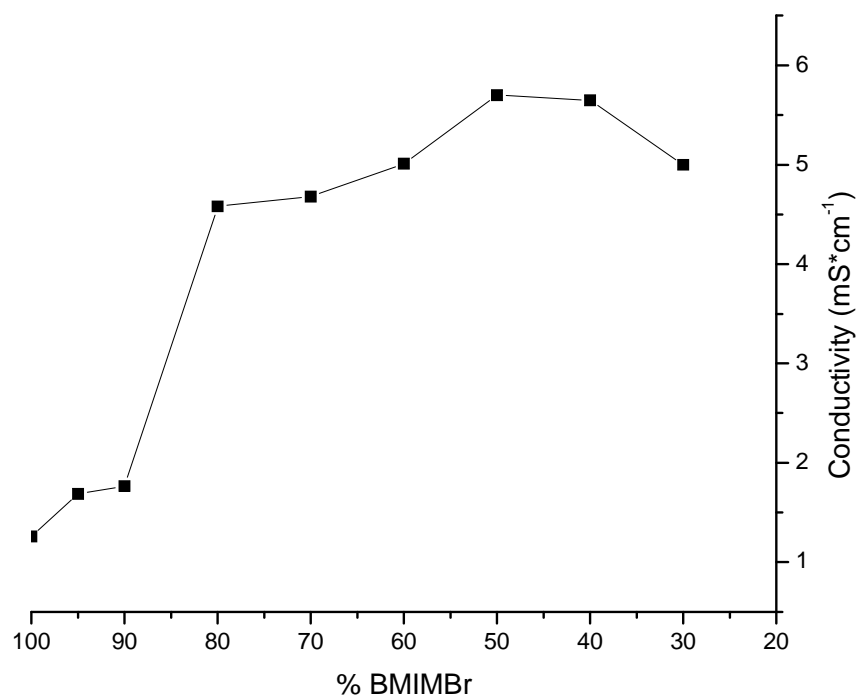


**Figure 3.5. Conductivity test of various percentage (in volume) of BMIMBr in CH<sub>2</sub>Cl<sub>2</sub>.**

From Figure 3.5, we observed that 100% pure ionic liquid has the lowest conductance, hence the highest resistance. Hence, the electrochemistry carried out showed that the current was passing through the ionic liquid and not the porphyrin sample added in there. This shows that the high viscosity and the large size ion reduced the ion mobility and average conductivities. As shown in Section 3.4.3, the best combination to carry out the electrochemistry experiment is to add 25% CH<sub>2</sub>Cl<sub>2</sub> was added into the RTIL. By adding CH<sub>2</sub>Cl<sub>2</sub>, the viscosity of the RTIL is reduced and at the same time enhanced the mass transport of analyte to the electrode surface is enhanced.

### 3.3.1.5. Dissolution of Co(II)TPP in BMIMBr

We had considerable difficulty trying to reduce/oxidize metalloporphyrins in our

SEC cell with RTILs. No charges were obtained with Soret band as the electrochemistry was being carried out. The initial peak of the Soret band observed is at 434nm. After searching the literature, we learned that the Soret band of Co(II)TPP should be at 410nm when CH<sub>2</sub>Cl<sub>2</sub> is the solvent. To understand the spectral changes, we added Co(II)TPP into CH<sub>2</sub>Cl<sub>2</sub> in a sealable UV cell and pumped under vacuum for approximately 20-30min. A UV-visible spectrum was then collected (results shown as black line in the Figure 3.6). The Co(II)TPP solution was then mixed with the IL which is isolated in a separated compartment of the UV cell. UV-visible spectra were collected every 5 minutes after mixing. The 410 nm peak gradually decreased as the 434 nm peak increased. After about 45-50 minutes, the 410 nm completely disappeared while a new peak at 434 nm appeared (result shown as the red line in Figure 3.6). This showed that the Co(II)TPP was oxidized by the ionic liquid to Co(III)TPP. This also helped to explain why the Co(II)/Co(III) oxidation and reduction peaks were never observed (usually around 100-500mV range).

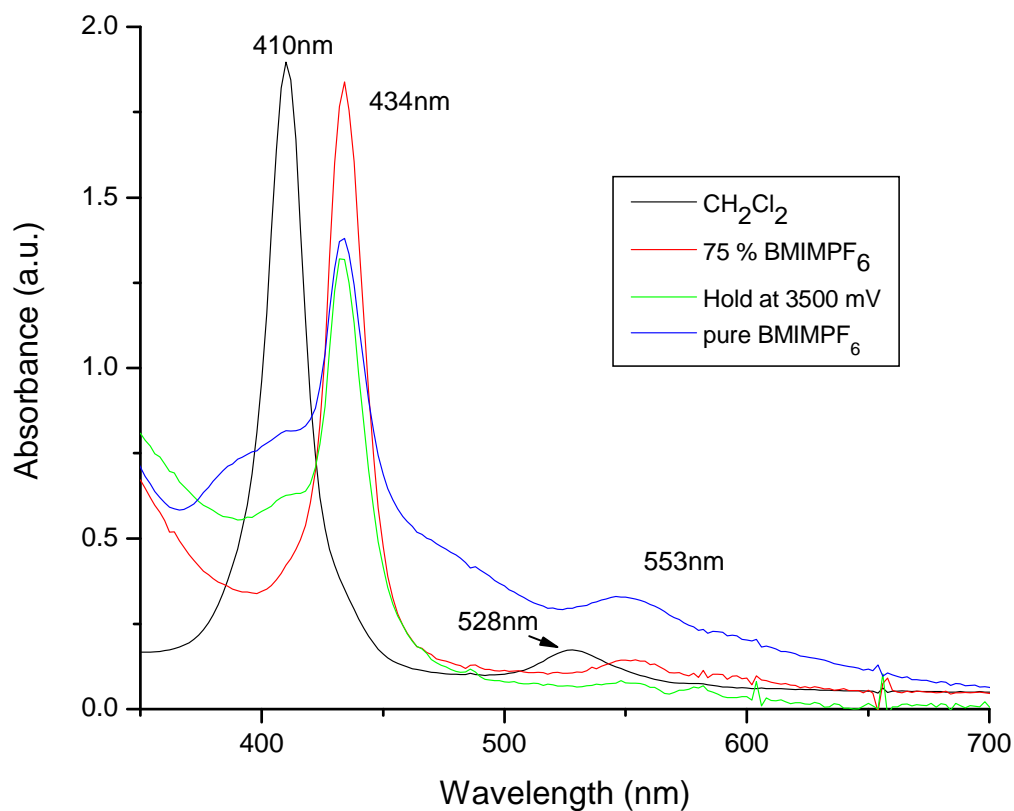


**Figure 3.6. UV-visible spectrum of Co(II)TPP in CH<sub>2</sub>Cl<sub>2</sub> (black line), after 70% BMIMPF<sub>6</sub> added for 30 minutes (red line), in mixture of 70% BMIMPF<sub>6</sub> and 25% CH<sub>2</sub>Cl<sub>2</sub> while holding the potential of the working electrode at 3500mV (green line), and in pure BMIMPF<sub>6</sub> (blue line).**

Reported in a literature<sup>[3]</sup> is the UV-visible spectra of Co(II)TPP undergoing oxidation. The results that we collected from the UV-visible spectra are close to the ones reported on the scheme shown in Section 1.1 (Scheme 1). We did observe the Soret band change from 410nm to 434 nm. However, for the Q bands we were only able to observe the 528nm band shifted to 553nm. This might be due to the low concentration of the Co(II)TPP or the interference of the electrodes placed in the spectroelectrochemistry



cell. The literature also reported the timed UV-visible spectra of the Co(II)TPP being oxidized through out the period of 7 hours (shown in Figure 1.1a). As the oxidation progresses from Co(III)TPP to Co(III)TPP<sup>+</sup>, the 448nm peak is suppressed as the 412nm peak becomes more visible. The same result (green line in Figure 3.6) was also being observed in our case. During the spectroelectrochemistry experiment, the potential was set at 3500mV while UV-visible spectrum was collected. Our result shows the 443nm peak decreased by roughly 30% while the 412nm peak emerged.

#### **3.3.1.6. Co(II)TPP oxidized by the ionic liquid under different temperature**

Since we learned that the Co(II)TPP was able to be oxidized by RTIL, one thing we would like to determine is if the oxidation was dependent on temperature. Up to this point, all the experiments were done are at room temperature (20°C). The same vacuum sealed oxidation experiments were done at 5 °C, 10 °C, and 15°C. Results collected are shown in the Figures 3.7a-d.

Figure 3.7a-d shows that the rate of oxidation reaction decreases in lower temperatures. By calculating the ratio of the changes according to the temperature, we can determine what order the oxidation process is.

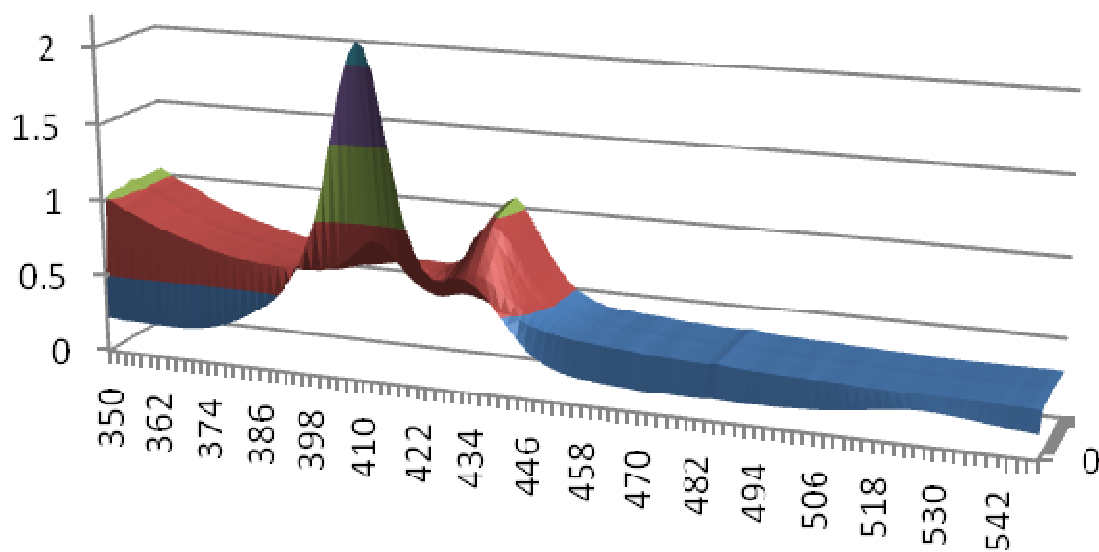


**Figure 3.7a.** Co(II)TPP oxidized by BMIMBr at 5°C.

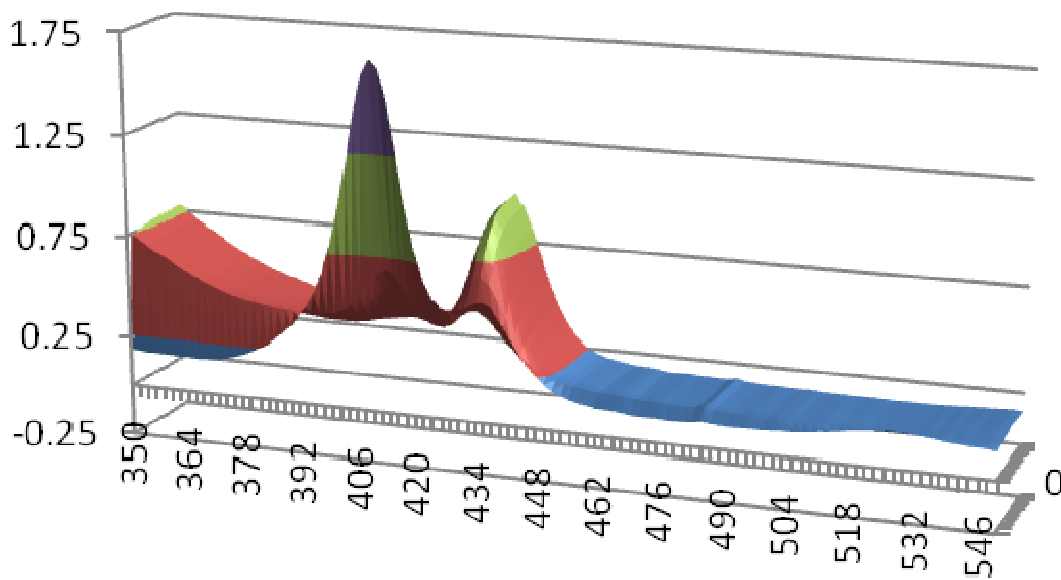


**Figure 3.7b.** Co(II)TPP oxidized by BMIMBr at 10°C.

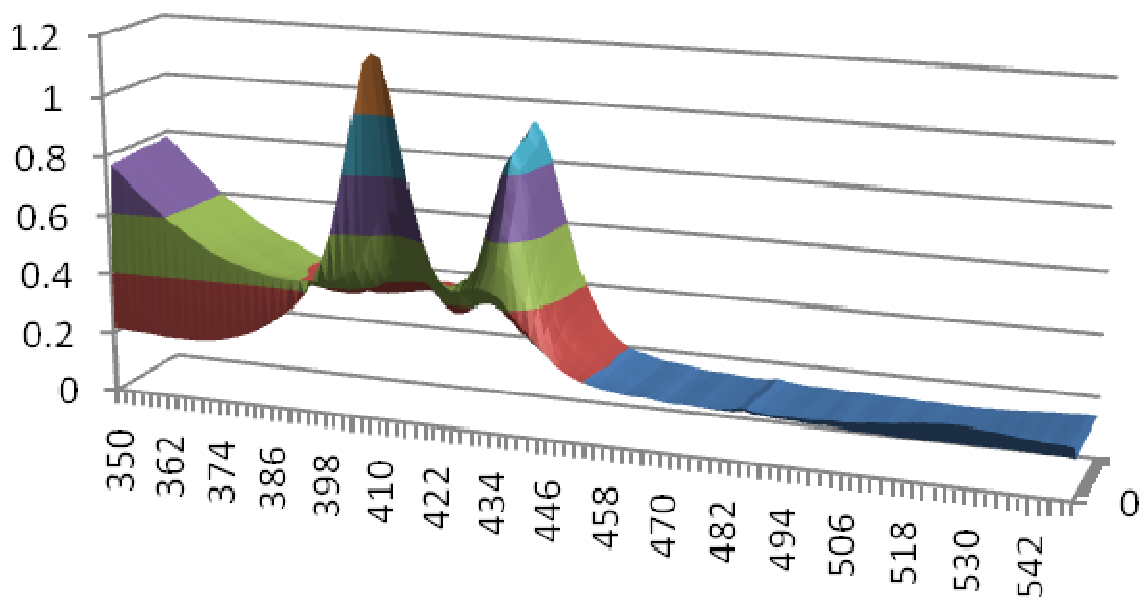


Figure 3.7c. Co(II)TPP oxidized by BMIMBr at 15°C.

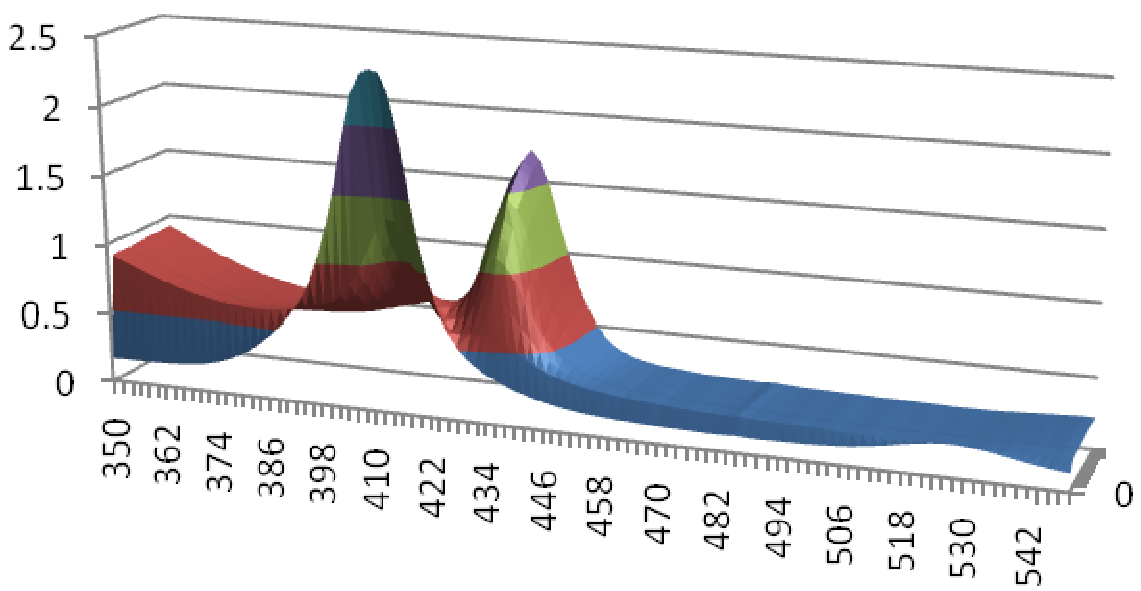
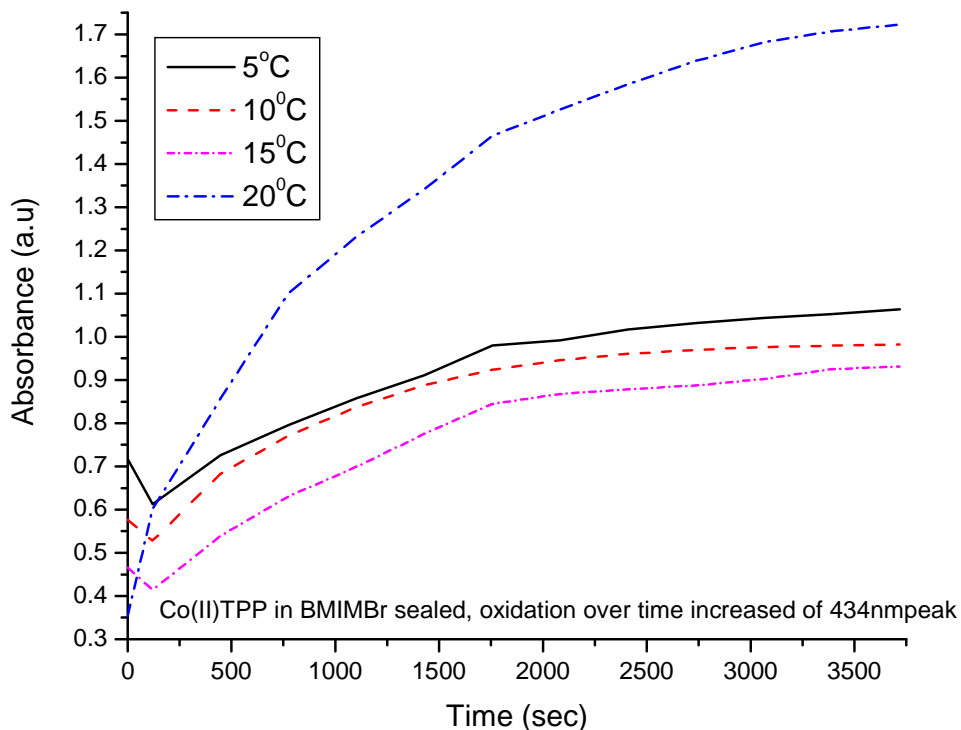


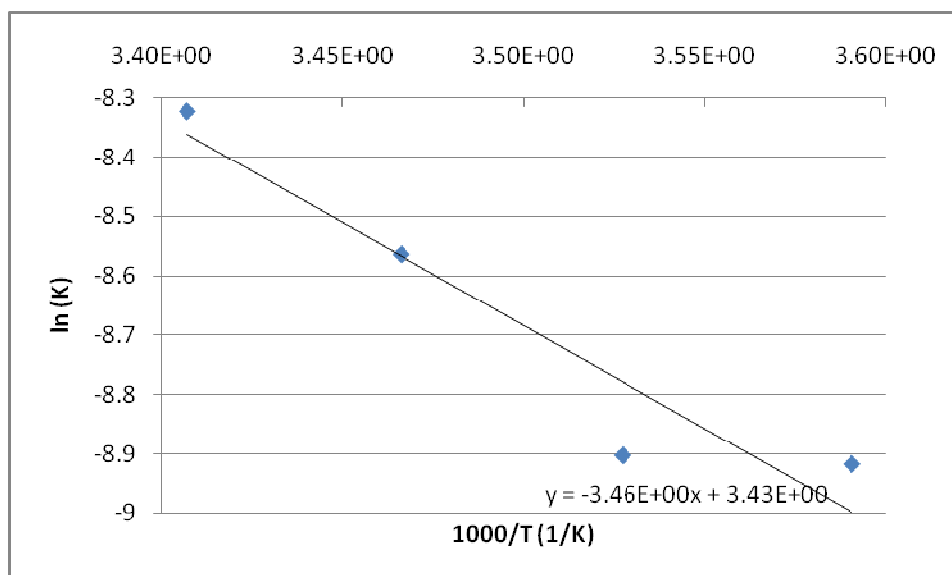
Figure 3.7d. Co(II)TPP oxidized by BMIMBr at 20°C.

Figure 3.8 below shows that the oxidation process of Co(II)TPP by the RTILs is temperature dependent.



**Figure 3.8. Absorbance change of 434nm peak of Co(II)TPP in BMIMBr at temperature held at 5, 10, 15, and 20°C.**

Figure 3.9 shows the Arrhenius plot obtained by measuring the rate constant  $k$  of the oxidation reaction of Co(III)TPP by the ionic liquid at different temperatures. The activation energy can be calculated by multiplying the slope of the line above by the negative value of the gas constant, which turns out to be 29 KJ/mol.



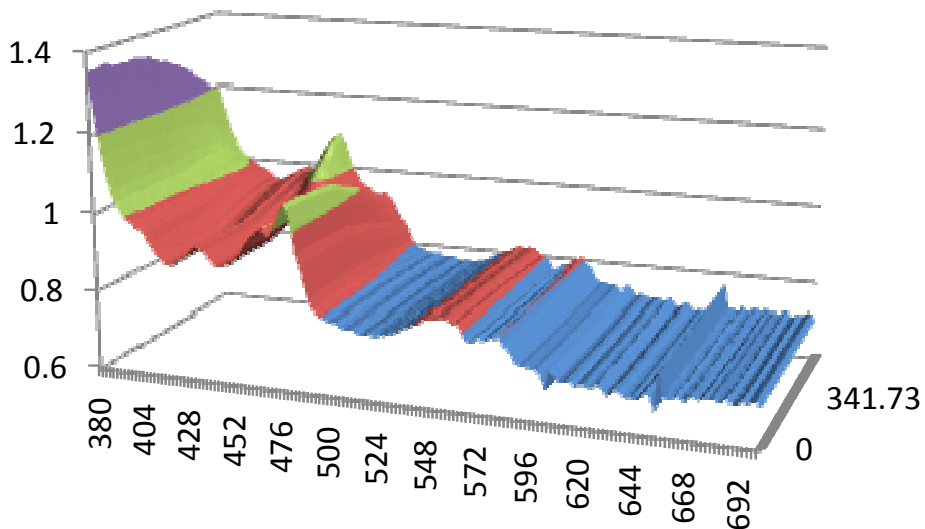
**Figure 3.9. Arrhenius plot of ln(K) vs 1/T.**

### 3.3.2. Studies done on Mn(III)TPPCl in ionic liquid

#### 3.3.2.1. Reduction

Studies on Mn(III)TPPCl in RTIL were also carried out in our laboratory. During our experiments, using RTIL as solvent, formation of six-coordinate Mn(III) species, such as Mn(III)TPPCl(L) and Mn(III)TPP(L)<sup>2+</sup>, and five-coordinate Mn(II) species, such as Mn(II)TPP(L), might exist in the solution<sup>[7]</sup>.

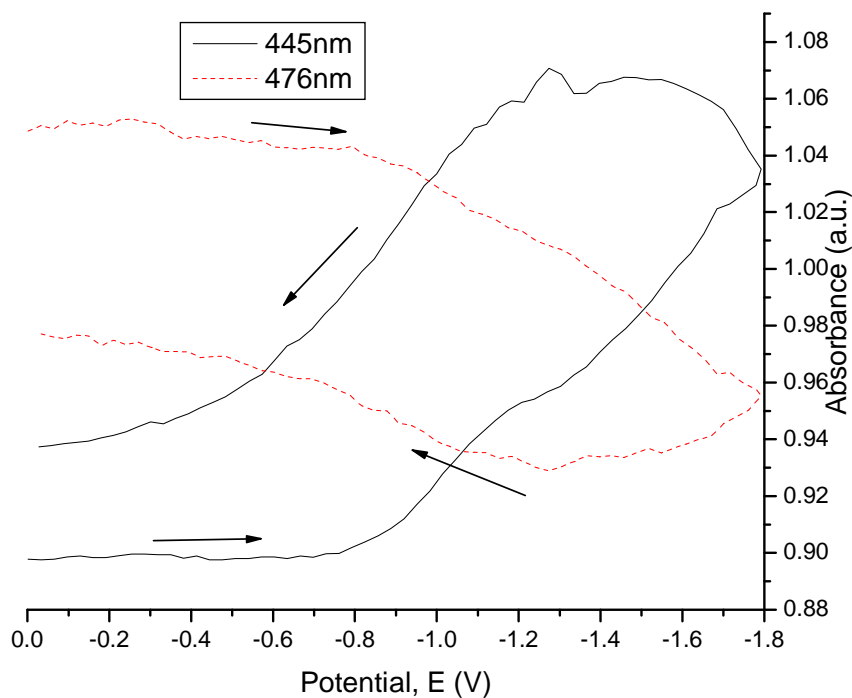
The results shown in the Figure 3.10 were obtained by using RTIL/CH<sub>2</sub>Cl<sub>2</sub> mixture as solvent. 0.02mM of Mn(III)TPPCl was added into a mixed solvent of 75% BMIMPF<sub>6</sub> and 25% CH<sub>2</sub>Cl<sub>2</sub>. UV-visible spectra were taken as the potential of the working electrode is increased from 0mV to -600mV at the rate of 1mV/s, with spectra taken roughly every 10 seconds. From the spectra, we can observe that the 476nm Soret band shifted to 442nm gradually which agree with the reported from literature shown in Figure 1.2<sup>[7]</sup>.



**Figure 3.10. UV-visible spectra of Mn(III)TPPcI while undergoing reduction.**

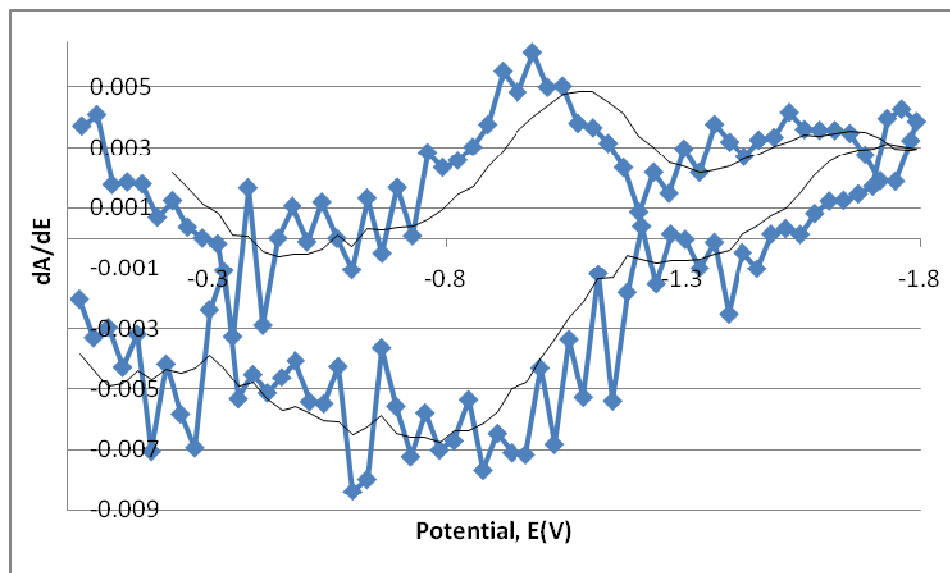
However, in the UV-visible spectra taken, we were also able to observe the Q band at 550 and 580nm. The ratio of the Q band and Soret band remains the same as it implied that the Cl<sup>-</sup> ion is still bound to the Mn metal center.

Figure 3.11 is the absorbance plot of the 476 nm Soret band vs the electrode potential. The 476 nm Soret band started to decrease and shifted to 445 nm as the electrode potential reached around -1V. As the potential swept back to 0mV, the 476 nm Soret band did not increase back to its original absorbance intensity. This either indicates that the re-oxidation process takes longer time or the Mn(II) did not fully oxidize back to Mn(III). The reason re-oxidation process takes longer time is due to the uncompensated resistance of the solvent. This phenomenon is not unexpected as ionic liquid was used as the solvent in our case.



**Figure 3.11. Reduction reaction of Mn(III)TPPCl.  $\lambda_{\max}$  vs E.**

Figure 3.12 below is the regenerated CV using the data collected from the UV-visible changes shown in Figure 3.11. The value of the potential gathered from the CV shown in Figure 3.12 is consistent to the ring reduction of the Mn metalloporphyrins which is usually around -1 V to -1.5 V<sup>[52]</sup>.



**Figure 3.12. Plot of  $\Delta A/\Delta E$  vs.  $E$ . Bold line is the raw data. Thin line is the smoothed data where two data points were averaged together.**

Figure 3.13 shown below is the CV collected during the spectroelectrochemical experiment of reduction reaction of Mn(III)TPPCl in BMIMPF<sub>6</sub>. The CV collected should show the reduction peak similar or close to the potential of the CV generated from the UV-visible spectra shown in Figure 3.12. However, in our experiment this does not seem to be the case. The reason the CV collected did not show the reduction peak at all is due to the background current of the ionic liquid. This can be observed in Figure 3.10 where the background around 380 nm was changing.



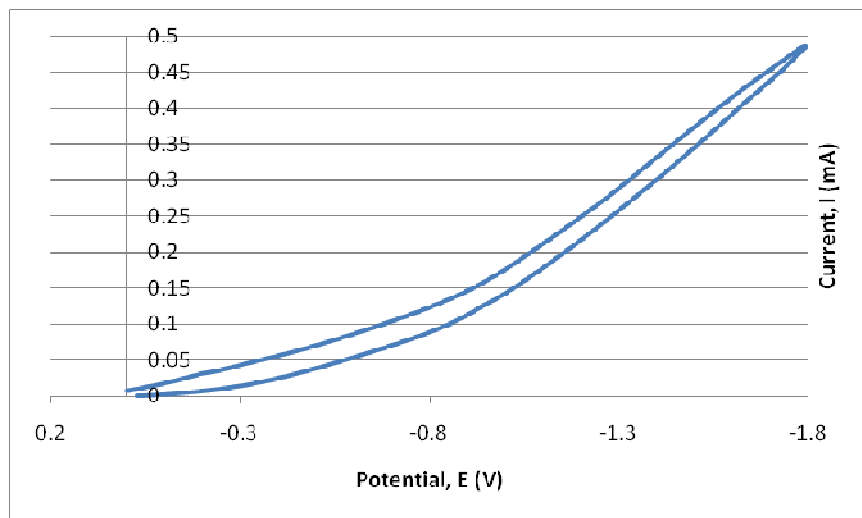


**Figure 3.13. CV of reduction reaction of Mn(III)TPPCl in BMIMPF<sub>6</sub>.**

### 3.3.2.2. Oxidation

Shown in Figure 3.14 is the UV-visible spectra changes of Mn(III)TPPCl during oxidation reaction. Result obtained is similar to the one shown in Figure 1.4. As the reduction reaction is carried out, the 476 nm band will decrease.

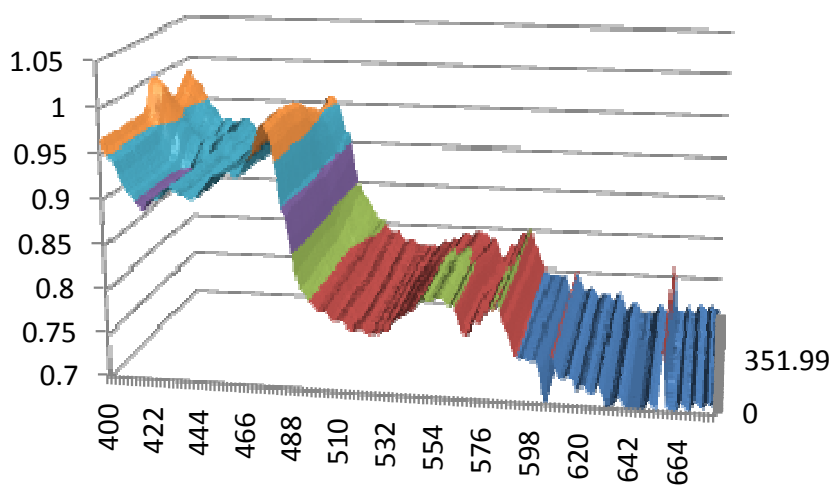


**Figure 3.14. UV-visible spectra of Mn(III)TPPCl while undergoing oxidation reaction.**

Figure 3.15 is the absorbance of the Soret band of Mn(III)TPPCl at 476 nm plot against the electrode potential. From the figure we observed that the Soret band decreased as the potential at the electrode increased. Upon reduction process, the absorbance of the 476 nm Soret band increased back to relatively close to the original absorbance. This shows that after the oxidation process, the Mn porphyrins do reduced back to Mn(III) complexes. The data collected is consistent to the one reported in literature shown in Figure 1.4.

From the Mn(III)TPPCl data obtained, we can conclude that Mn(III)TPPCl is not oxidized or reduced by RTIL as solvent. Since Fe(III)TPPCl have the similar behavior, we would expect the same results as Mn(III)TPPCl.

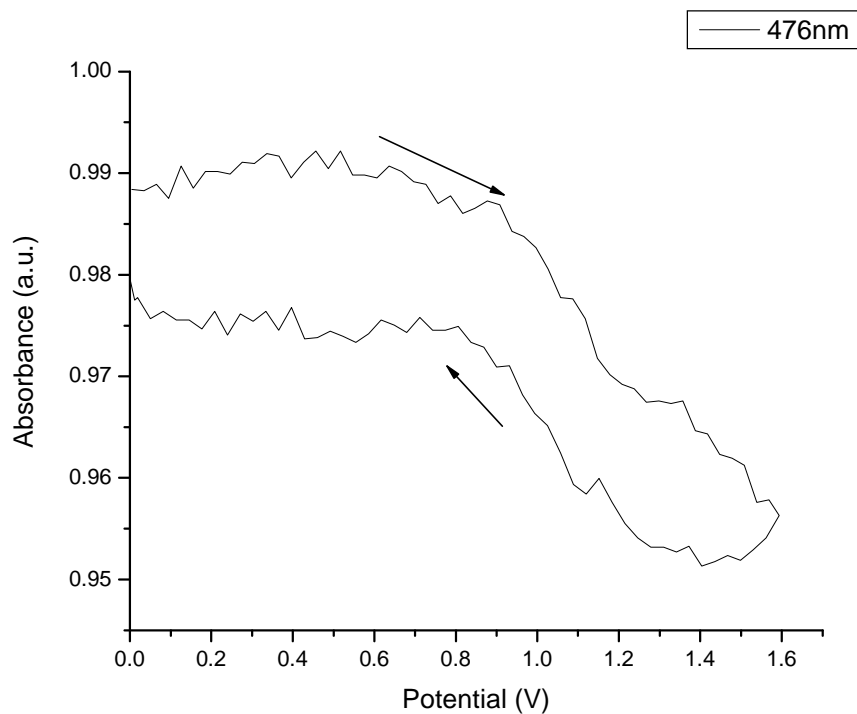


**Figure 3.15. Oxidation reaction of Mn(III)TPPCl.  $\lambda_{\max}$  vs E.**

### **3.3.3. Studies done on Fe(III)TPPCL in ionic liquid**

#### **3.3.3.1. Fe(III)TPPCL reduced by ionic liquid**

Figure 3.16 shows the UV-visible spectra changes of Fe(III)TPPCL being reduced by BMIMBr. Reduction of Fe<sup>III</sup> to Fe<sup>II</sup> porphyrin by anionic ligands and good bases is well known in the metalloporphyrin literatures [7, 8, 51, 53]. Usually halides do not do this reaction, but, as part of the solvent, the reaction may be fast enough. The 418nm Soret band decreased in absorbance as the Soret band at 431nm increased in absorbance over time as the RTIL is added into the solution. We also observed the disappearance of the Q band 511 nm and were being replaced by the 537nm Q band. This suggested that as the Fe<sup>III</sup> is reduced to Fe<sup>II</sup>, the anion of the RTIL is interacting with the porphyrin as a new ligand. This reaction is not uncommon for high coordination metal such as iron.

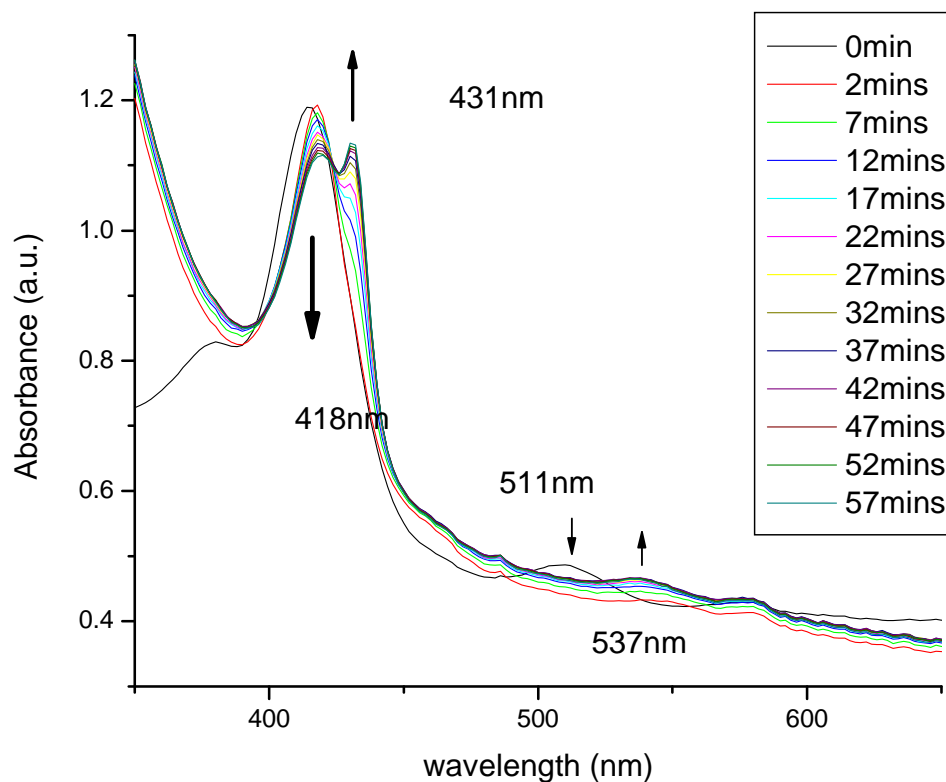


**Figure 3.16 UV-visible spectra of Fe(III)TPPCl being reduced by BMIMBr. Spectra were taken every 5 minutes in a vacuum sealed UV cell.**

### 3.3.3.2. Fe(III)TPPCl further reduced by electrochemistry

Spectroelectrochemical experiments were also done on Fe(III)TPPCl in RTIL. From Section 3.3.3.1, we found that the Fe(III)TPPCl is able to be oxidized by the RTIL. A time dependent UV-visible spectra changes were obtained during the controlled potential reduction of Fe(III)TPPCl in RTIL. The result is shown in Figure 3.17. The potential of the working electrode was held at -1700mV. The changes in the UV-visible spectra are similar to the time dependent UV-visible spectra of Fe(III)TPPCl being reduced by RTIL shown in Figure 3.16. The difference between these two experiments is by holding the working electrode's potential at -1700mV, the reduction is faster

compared to the reduction by the ionic liquids. The spectra gather (Figure 3.17) agree with those reported in literatures in Section 1.1. This concludes that upon addition of the RTIL into the Fe(III)TPPCl, iron(III) is reduced to four coordinated Fe(II)TPP along with a five-coordinated iron(II) complex. When the potential of the electrode is held beyond the reduction potential, only the five-coordinated iron(II) complex is observed. This is due to the counter ions in the RTIL help to stabilize the five-coordinated iron porphyrins.

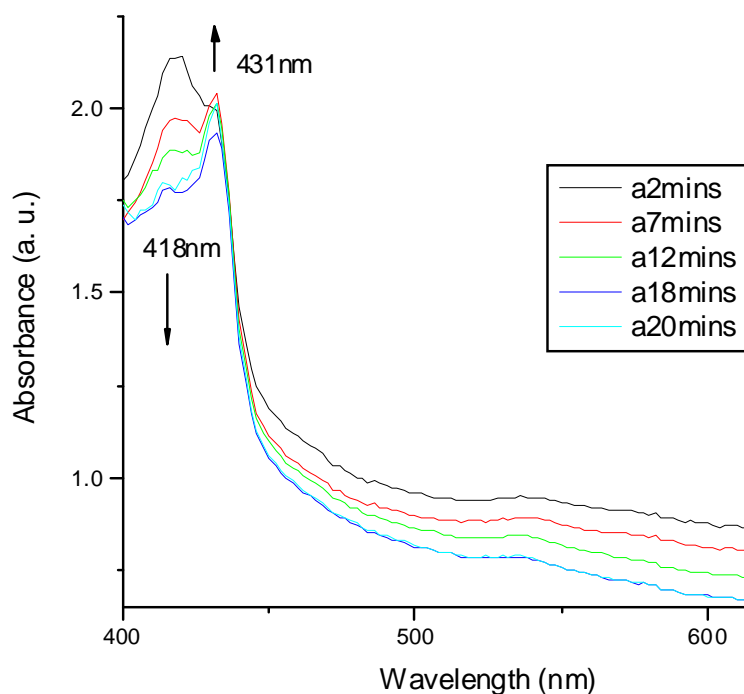


**Figure 3.17. Time-dependent UV-visible spectra changes obtained during the controlled-potential reduction of Fe(III)TPPCl in BMIMBr.**

Figure 3.16 shows the Soret band at 418 nm and 431 nm along with the Q band at 537nm are consistent with the data shown in Table 1.1. These bands are assigned to the four coordinated Fe(II)TPP. As the electrode potential was held at -1700mV, the only band that was observed were the Soret band at 431 nm and the Q band at 537 nm. From

the Table 1.1 we can conclude that the majority of the species in the solution when the electrode potential was hold at -1700mV was  $[\text{Fe(II)TPPCl}]^-$ . However, due to the low concentration of the sample used, it is reasonable to assume that the 570 nm and 610 nm bands were too weak to be observed. Another explanation of why the 570 nm and 610 nm bands were not observed is shown in Figure 3.18.

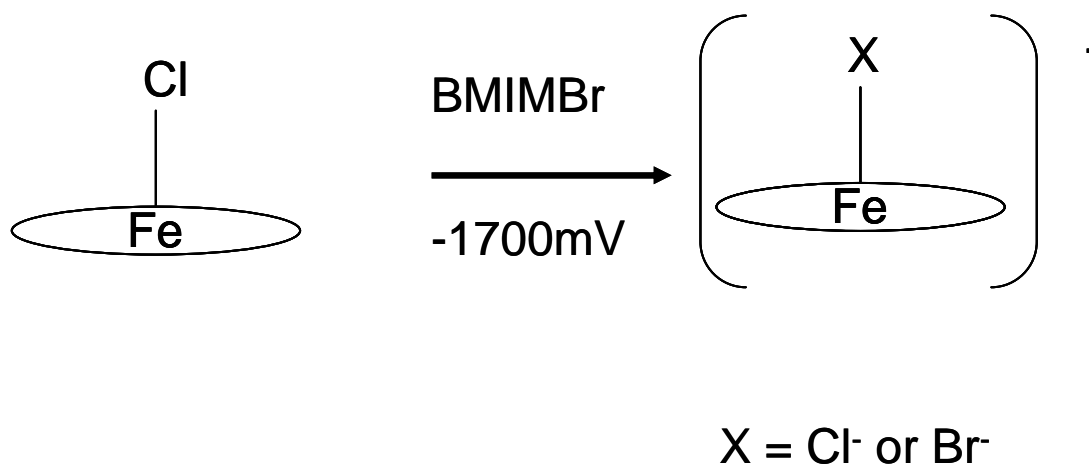


**Figure 3.18. Scheme of the prediction of the reduction of Fe(III)TPPCl.**

Figure 3.18 is a proposed scheme of reduction of Fe(III)TPPCl in BMIMBr. As the Fe(III)TPPCl is dissolved in the ionic liquid, the porphyrin is being reduced to Fe(II)TPP and was stabilized by the ion in the ionic liquid. Since the  $\text{Br}^-$  is much more abundant in the ionic liquid compare to the  $\text{Cl}^-$  dissociated from the Fe(III)TPPCl. As Le Chatelier's principle suggested, there is a good possibility that  $\text{Br}^-$  is associated with the iron(II) center rather than  $\text{Cl}^-$ . Due to that  $\text{Br}^-$  is much bulkier than  $\text{Cl}^-$ , the interaction between the halide and iron center is weaker. This could explain some of the Q bands were too weak to be observed.

## IV. Conclusion

Ionic liquids based on imidazolium cation and two different anions have been used in spectroelectrochemistry studies. The low melting point, low viscosity, and high conductivity, which are the desired properties for an ionic liquid, appear to depend on the following requirements. Both the anion and the cation must be small and bear a well-delocalized charge, and symmetry of the imidazolium cation is to be avoided for low melting points<sup>[35]</sup>.

From the results obtained, we found that RTIL is reasonably good for using as solvent in spectroelectrochemical experiment. The major problem with using RTIL as solvent is the viscosity of the RTIL which leads to low conductivity of the analyte. However, the issue can be resolve by adding a small portion of  $\text{CH}_2\text{Cl}_2$  into the solvent. Another way to dissolve the porphyrins in pure RTIL is to put the mixture in an ultrasonic cleaner. Although most RTILs are hydrophobic; some RTILS are known to dissolve water from the atmosphere.

From all the electrochemical experiments collected using RTIL as solvent, we come to conclusion that RTIL can be used as a solvent during a electrochemical experiments. The redox reactions of metalloporphyrins behave similar to those done in conventional solvent/electrolyte solutions. By using RTILS, one is able to eliminate the used of electrolyte where contamination could interfere with the experiments and costly. RTILs are more environmental friendly as they can be recycled after each experiment; this will minimized the production of chemical waste significantly.

Since RTILs are not typical conventional solvents, they do possess some unconventional properties that lead to a few phenomena that required our attention. The initial problem we encountered is the solubility problem of the analyte in the ionic liquids. Porphyrin complexes were added into the ionic liquid and need to be stirred vigorously and degassed for 12 to 24 hours before the UV-visible spectral or CV can be taken. Aside from the dissolution problem, we also encountered the conductivity issue. Although in ionic liquid, where ions are abundant and more than sufficient to transfer charges, the resistance was high enough that complete electrolysis across the working electrode surface could not be observed. As a result, the redox peaks of the analyte observed in the CV were difficult to observe. The same problem also occurs when the spectroelectrochemical experiment was carried out, with insufficient electrolysis in the spectral window. As the electrode potential increases, the baseline of the UV-visible spectra increases as well.

In order to overcome this issue, we decided to create a mixture of ionic liquid with  $\text{CH}_2\text{Cl}_2$ . This will enable us to dissolve the analyte faster. And by adding  $\text{CH}_2\text{Cl}_2$  into the ionic liquid, the viscosity of the solvent was decreased. When the conductivity test was carried out on various mixtures of  $\text{CH}_2\text{Cl}_2$  and ionic liquid, we found that as the amount of  $\text{CH}_2\text{Cl}_2$  increases, the conductivity of the solvent increases. As a result, when redox reactions were carried out in the CV, we found that more current was able to pass through the solution<sup>[17, 53]</sup>. Hence, we are able to obtain decent CV and were able to observe the UV-visible spectral changes during the spectroelectrochemical experiment.



Addition of solvent like  $\text{CH}_2\text{Cl}_2$  helped to break up the aggregation of the ionic liquid. Loss of aggregation in the ionic liquid enabled higher diffusion, and lead to more currents being able to pass through the analyte instead of into the ionic liquid.

## References

- [1] A. A. Krasnovskii, *Ann. Rev. Plant Physiol.* **1960**, *11*, 363.
- [2] in *McGraw-Hill Concise Encyclopedia of Bioscience.*, Vol. The McGraw-Hill Companies, Inc, **2002**.
- [3] W. Nam, W. Hwang, S. J. Baek and B. C. Sohn, *Bull. Korean Chem. Soc.* **1995**, *16*, 896.
- [4] M. C. Lagunas, D. S. Silvester, L. Aldous and R. G. Compton, *Electroanalysis* **2006**, *18*, 2263-2268.
- [5] K. M. Smith, Ed., *Porphyrins and Metalloporphyrins*, Elsevier, Amsterdam, **1975**, p.
- [6] D. H. Jones and A. S. Hinman, *J. Chem. Soc. Dalton Trans.* **1992**, 1503-1508.
- [7] X. H. Mu and F. A. Schultz, *Inorg. Chem.* **1995**, *34*, 3835-3837.
- [8] X. H. Mu and F. A. Schultz, *Inorg. Chem.* **1992**, *31*, 3351-3357.
- [9] L. A. Bottomley and K. M. Kadish, *Inorg. Chem.* **1981**, *20*, 1348-1357.
- [10] F. Paulat and N. Lehnert, *Inorg. Chem.* **2008**, *47*, 4963-4976.
- [11] P. K. Shantha, H. H. Thanga and A. L. Verma, *J. Raman Spectrosc.* **1998**, *29*, 997-1001.
- [12] K. M. Kadish and L. A. Bottomley, *Inorg. Chem* **1980**, *19*, 832-836.
- [13] K. M. Kadish, L. A. Bottomley, S. Kelly, D. Schaeper and L. R. Shiue, *Bioelectrochem. Bioenerg.* **1981**, *8*, 213-222.
- [14] C. Hu, B. C. Noll and W. R. Scheidt, *Inorg. Chem* **2007**, *46*, 8258-8263.

- [15] J. P. Collman, J. I. Brauman, K. M. Dexsee, T. R. Halbert, E. Bunnenberg, R. E. Linder, G. N. LaMar, J. D. Gaudio, G. Lang and K. Spartalian, *J. Am. Chem. Soc* **1980**, *102*, 4182-4192.
- [16] F. A. Walker, M.-W. Lo and T. Ree, *J. Am. Chem. Soc* **1976**, *98*, 5552-5560.
- [17] K. M. Kadish and R. K. Rhodes, *Inorg. Chem* **1983**, *22*, 1090-1094.
- [18] E. I. Rogers, D. S. Silvester, D. L. Poole, L. Aldous, C. Hardacre and R. G. Compton, *J. Phys. Chem. C* **2008**, *112*, 2729-2735.
- [19] D. B. Zhao, M. Wu, Y. Kou and E. Min, *Catal. Today* **2002**, *74*, 157-189.
- [20] T. Welton, *Coord. Chem. Rev.* **2004**, *248*, 2459-2477.
- [21] Z. P. Rosol, N. J. German and S. M. Gross, *Green Chem.* **2009**, *11*, 1453-1457.
- [22] D. Q. Shi, Y. Zhou and S. F. Rong, *Synth. Commun.* **2009**, *39*, 3500-3508.
- [23] N. Tachikawa, Y. Katayama and T. Miura, *Electrochem. Solid-State Lett.* **2009**, *12*, F39-F41.
- [24] J. M. Zhang, C. H. Yang, Z. S. Hou, B. X. Han, T. Jiang, X. H. Li, G. Y. Zhao, Y. F. Li, Z. M. Liu, D. B. Zhao and Y. Kou, *New J. Chem.* **2003**, *27*, 333-336.
- [25] J. S. Wilkes, J. A. Levisky, R. A. Wilson and C. L. Hussey, *Inorg. Chem.* **1982**, *21*, 1263-1264.
- [26] A. M. O'Mahony, D. S. Silvester, L. Aldous, C. Hardacre and R. G. Compton, *J. Chem. Eng. Data* **2008**, *53*, 2884-2891.
- [27] T. L. Broder, D. S. Silvester, L. Aldous, C. Hardacre and R. G. Compton, *J. Phys. Chem. B*, **2007**, *111*, 7778-7785.
- [28] S. Zhang, N. Sun, X. He, X. Lu and X. Zhang, *J. Phys. Chem. Ref. Data* **2006**, *35*, 1475-1517.

- [29] D. S. Silvester, L. Aldous, C. Hardacre and R. G. Compton, *J. Phys. Chem. B* **2007**, *111*, 5000-5007.
- [30] A. M. O'Mahony, D. S. Silvester, L. Aldous, C. Hardacre and R. G. Compton, *J. Phys. Chem. C* **2008**, *112*, 7725-7730.
- [31] H. Weingartner, P. Sasisanker, C. Daguene, P. Dyson, I. Krossing, J. Slattery and T. Schubert, *J. Phys. Chem. B* **2007**, *111*, 4775-4780.
- [32] E. I. Rogers, D. S. Silvester, D. L. Poole, L. Aldous, C. Hardacre and R. G. Compton, *J. Phys. Chem. C*, **2008**, *112*, 2729-2735.
- [33] B. D. Fitchett, T. N. Knepp and J. C. Conboy, *J. Electrochem. Soc.* **2004**, *151*, E219-E225.
- [34] J. G. Huddleston, A. E. Visser, W. M. Reichert, H. D. Willauer, G. A. Broker and R. D. Rogers, *Green Chem.* **2001**, *3*, 156-164.
- [35] P. Bonhote, A.-P. Dias, N. Papageorgiou, K. Kalyanasundaram and M. Gratzel, *Inorg. Chem* **1996**, *35*, 1168-1178.
- [36] O. O. Okoturo and T. J. VanderNoot, *J. Electrochem. Soc.* **2004**, *568*, 167-181.
- [37] K. R. Seddon, A. Stark and M. J. Torres, *ACS Symp. Ser.* **2002**, *819*, 34-39.
- [38] A. B. McEwen, E. L. Ngo, K. LeCompte and J. L. Goldman, *J. Electrochem. Soc.* **1999**, *146*, 1687-1695.
- [39] Y. Hu, Z. Wang, H. Li, X. Huang and L. Chen, *J. Electrochem. Soc.* **2004**, *151*, A1424-A1428.
- [40] N. Ignat'ev, U. Welz-Biermann, A. Kucheryna, G. Bissky and H. Willner, *J. Fluorine Chem.* **2005**, *126*, 1150-1159.
- [41] A. B. McEwen, S. F. McDevitt and V. R. Koch, *J. Electrochem. Soc.* **1997**, *144*, L84.

- [42] M. Badri, J.-J. Brunet and R. Perron, *Tetrahedron Lett.* **1992**, 33, 4435.
- [43] J. A. Widegren, E. M. Saurer, K. N. Marsh and J. W. Magee, *J. Chem. Thermodyn.* **2005**, 37, 569-575.
- [44] U. Schroder, J. D. Wadhawan, R. G. Compton, F. Marken, P. A. Z. Suarez, C. S. Consorti, R. F. de Souza and J. Dupont, *New J. Chem.* **2000**, 24, 1009-1015.
- [45] M. C. Buzzeo, C. Hardacre and R. G. Compton, *Chem. Phys. Chem.* **2006**, 7, 176-180.
- [46] S. V. Dzyuba and R. A. Bartsch, *J. Heterocycl. Chem.* **2001**, 38, 265-268.
- [47] P. A. Z. Suarez, S. Einloft, J. E. L. Dullius, R. F. de Souza and J. Dupont, *J. Chim. Phys. Phys.-Chim. Biol.* **1998**, 95, 1626-1639.
- [48] J. G. Huddleston, A. E. Visser, W. M. Reichert, H. D. Willauer, G. A. Broker and R. D. Rogers, *Green Chem.* **2001**, 3, 156-164.
- [49] M. A. Phillipi and H. M. Goff, *J. Am. Chem. Soc.* **1982**, 104, 6026-6034.
- [50] N. Carnieri and A. Harriman, *Inorg. Chim. Acta* **1982**, 62, 103-107.
- [51] J.-H. Fuhrhop, K. M. Kadish and D. G. Davis, *J. Am. Chem. Soc.* **1973**, 95, 5140.
- [52] F. D'Souza, P. Boulas, A. M. Aukauloo, R. Guilard, M. Kisters, E. Vogel and K. M. Kadish, *J. Phys. Chem.* **1994**, 98, 11885-11891.
- [53] Y. Liu and M. D. Ryan, *J. Electroanal. Chem.* **1994**, 368, 209-219.